OPTIMIZATION AND VALIDATION OF PUMPING SYSTEM DESIGN AND OPERATION FOR WATER SUPPLY IN HIGH-RISE BUILDINGS

TIM M. MÜLLER, PHILIPP LEISE, IMKE-SOPHIE LORENZ, LENA C. ALTHERR, AND PETER F. PELZ

Abstract. The application of mathematical optimization methods provides the capacity to increase the energy efficiency and to lower the investment costs of technical systems, considerably. We present a system approach for the optimization of the design and operation of pumping systems and exemplify it by applying it to the water supply of high-rise buildings. The underlying fluid system is modeled as a Mixed-Integer Nonlinear Program as well as a Mixed-Integer Linear Program by piecewise linearization of the pumps' characteristic curves. We consider layout and control decisions for different load scenarios, which leads to a two-stage stochastic optimization program. Besides the solution of the Mixed-Integer Nonlinear or Linear Program with off-the-shelf solvers, we implemented a problem specific algorithm to improve the computation time for solving the different models. Focusing on the efficient exploration of the solution space we divide the problem into smaller subproblems, which partly can be cut off in the solution process. On the one hand, we discuss the performance and applicability of the solution approaches for real buildings. On the other hand, we analyze the technical aspects of the solutions from an engineer's point of view. Furthermore, the constructed modular pumping test rig allows us to validate the optimization models experimentally and thus confirm the methodology.

1. Introduction

More than half of the world's population (55 %) lived in urban areas in 2018, as shown in UN [2018]. Based on this data published by the United Nations, it is estimated that 2.5 billion people will be added to the urban population by 2050. This continuous trend towards urbanization will lead to an increasing number of mega-cities with more than 10 million inhabitants.

Key components of any urban infrastructure are water supply systems, cf. Coelho and Andrade-Campos [2014], and urbanization will pose increasing challenges for these infrastructures in the future: Whilst a secure supply of water for the growing number of citizens is to be ensured, energy consumption for water supply must be reduced on the way to a more sustainable future. Thus, efficiency optimization of water supply systems has been in the focus of ongoing research, for a review cf. e.g. Coelho and Andrade-Campos [2014].

Date: October 2019.

Key words and phrases. Technical Operations Research, MINLP, MIP, Experimental Validation, Pumping Systems, Water Supply Systems.

While existing research has so far tended to focus on the energy consumption of larger centralized water infrastructures, in this contribution, we want to investigate the energy consumption of distributed pressure boosting pumping stations. These systems, also called booster stations, are installed in buildings and employed to supply the higher pressure zones with water. Especially in tall buildings, booster stations have a considerable energy consumption, in particular if they are wrongly dimensioned and/or operated.

As the space for living in cities is limited, with increasing urbanization also an increase in the number of high-rise buildings, and thus an increase of needed booster stations, is expected. Already today there is an exponential growth of completed buildings of 200 meters or greater height, CTBUH [2018]. In these tall buildings, the potential for energy savings through the application of several pressure zones or a decentralized pump placement and an optimal selection of pump types is high, cf. e.g. Altherr et al. [2019].

In order to unlock this optimization potential, a large number of pipe network topologies and pump configurations must be considered in the planning process. However, with the increasing number of degrees of freedom, especially in tall buildings, it is a great challenge to investigate all possible system variants, as the number of possible design choices can be overwhelming. Moreover, one not only has to check whether a promising design is able to fulfill the different load scenarios occurring in the building, but also has to weigh investment costs and operating costs against each other. To achieve these goals, we present an optimization-aided system design approach based on sophisticated algorithms. In order to ensure that the underlying optimization models represent the system under consideration with sufficient accuracy, we also present an experimental validation using different data sources for the models.

In the following Sec. 2, we introduce relevant literature for the optimization. Afterwards, we present the technical application in detail and show different formulations of the optimization model as well as a problem specific solving algorithm. We then discuss the performance of different solving approaches as well as technical aspects of the solutions and close with an experimental validation. Finally we draw a conclusion and give an outlook for future work.

2. Related Work

In this article we present a holistic approach to the optimal synthesis of technical systems, which we illustrate by means of a pumping system for water supply. In the context of this research focus, the state-of-the-art must therefore be presented in two different areas:

(i) Methods for the design and efficiency optimization of pumping systems, in particular pressure boosting systems in buildings.
(ii) Application of mathematical optimization methods to technical systems, in particular methods for two-stage optimization problems.

In the next two subsections we will give a short overview over relevant literature in these two areas.

2.1. **Design and Efficiency Optimization of Pumping Systems.** Centrifugal Pumps are commonly used for the transport of drinking water. Therefore, we focus on this pump type within this literature overview.

The development and hydraulic optimization of centrifugal pumps is already at a very high level, and multiple standard works are focusing on centrifugal pump design and performance, cf. e.g. Japikse et al. [1997], Brennen [2011], or Gülich [2013]. In recent decades, also through the use of computer-aided methods such as Computational Fluid Dynamics (CFD), cf. e.g. Garg [1998], the efficiency of centrifugal pumps, in particular at their design point, could be continuously improved.

In real life applications, however, it can be seen that pumps are predominantly operated in the partial load range for a large part of the time, cf. Hirschberg [2014]. In this case, the excess energy is either dissipated via throttling valves, or – if variable speed pumps are employed – they are operated at a lower rotational speed than their nominal rotational speed. Both leads to an operation at lower efficiency, often far away from their best efficiency point. Therefore when classifying pump performance, a suitable approach for assessing efficiency in practical usage is crucial.

The product approach, which is part of an European Standard for energy-efficiency evaluation of water pumps, c.f. EN 16480:2016, is a first step towards this direction. This approach no longer considers merely the pump as a component, but the pump and electric motor as part of a system. The efficiency of this system is assessed according to the Minimum Energy Efficiency Index (MEI) which rates the pump's efficiency not only at its design point, but also at partial load and overload. Therefore, the so-called "house of efficiency" scheme is applied, which sets efficiency criteria for 75%, 100% and 110% of the volume flow at the design point.

While this is a first step towards the right direction, in a real building does not solely vary the volume flow, but so does the required pressure increase in relation to it. In addition, when assessing overall energy efficiency, it is important to take into account the proportion of time of the different load requirements. For this reason, the Extended Product Approach, cf. Stoffel [2015], was developed within the scope of energy efficiency guidelines of the European Union. It considers a load profile which links volume flow and pressure demands, and gives corresponding time profiles. The energy consumption of the Extended Product (pump and electric motor) considering these load profiles then yields the Energy Efficiency Index (EEI), cf. Lang et al. [2013].

Also with a system-wide assessment in mind, the scope of the international Standard "Pump system energy assessment" is to set "the requirements for conducting and reporting the results of a pumping system energy assessment [...] that considers the entire pumping system, from energy inputs to the work performed as the result of these inputs", ISO/ASME 14414. However, it does not specify how to design a pumping system or how to validate the energy savings that would result from implementing recommendations based on this assessment, cf. ISO/ASME 14414, two aspects that we cover in this work.

The Standards DIN 1988-500 and DIN 1988-300 provide codes of practice for drinking water installations. While DIN 1988-500 focuses on the dimensioning of pressure boosting systems with RPM-regulated pumps, DIN 1988-300 describes the dimensioning of the pipe network. Particularly, the selection of suitable pipe diameters in regard to restrictions such as a peak load volume flow and a maximal water velocity for reasons of noise is set out. In addition to a central configuration, the Standard DIN 1988-500 also considers some decentral configurations due to the specification of different pressure zones within the building. For example, lower pressure zones of the building can be supplied directly by the public water mains and solely higher pressure zones are supplied via a pressure boosting system. In addition, the installation of several pressure boosting systems is described so that each pressure zone is supplied by its own pumping system. However, more sophisticated decentralized configurations, which could be automatically assessed and evaluated by our approach, are not considered.

In general there are different, system-wide measures to increase the energy efficiency of pumping systems:

- The optimal selection of pumps, i.e., usage of variable-speed pumps, cf. Ferreira et al. [2010], and avoiding over-dimensioning, cf. e.g. Fisher [2001], Tindall and Pendle [2015], Weber and Lorenz [2017, 2018].
- The allocation of several pressure zones within the building and the usage of decentralized pump layouts, cf. e.g. Norgaard and Nielsen [2010], Leise and Altherr [2018].
- The optimization of the pumps' operation, cf. e.g. Pedersen and Yang [2008], Groß et al. [2017], Nowak et al. [2018].

The approach presented in this contribution allows in principle to cover all three of these aspects, since not only the optimal pumping system design, but also its optimal operation can be considered. Furthermore, next to these efficiency consideration other possible objectives are shown in the literature. One example is the optimization of resilient water supply networks as shown by Herrera et al. [2016], Hartisch et al. [2018], Altherr et al. [2019].

2.2. **Mathematical Aspects of Two-Stage Optimization Problems in Engineering.** When designing an optimal pumping system, the overall goal often is to minimize the sum of investment costs and energy costs for the expected life cycle. Since the load within residential buildings varies, cf. Sec. 2.1 and Hirschberg [2014], its operation at different load points has to be considered to assess the energy costs of the pumping system.

The corresponding mathematical optimization problem consists of two stages: First, finding a low-priced investment decision, i.e. a pump and pipe configuration. Secondly, operating a subset of the pumps for each quasi-stationary demand of the load profile, such that the system satisfies this demand and the efficiency is maximized.

In this case, the considered load profile can be seen as a discrete distribution of uncertain load parameters, with the time portion of each load scenario corresponding to its probability of occurrence. The optimization

program which minimizes investment costs as well as expected value of operation costs can then be seen as the Deterministic Equivalent of a general two-stage stochastic program with recourse, cf. e.g. Wets [1974].

As many optimization problems in the area of engineering design are subject to uncertain parameters, e.g. uncertain material characteristics or load scenarios, two-stage stochastic programs have been frequently studied in this context, and a good overview can be found in Popela [2010] and Popela et al. [2014].

An important aspect for the difficulty of solving these two-stage optimization problems to global optimality is whether integer variables are (i) present in the first stage solely, or (ii) also present in the second stage.

Regarding design and operation optimization of technical systems, integer variables, and more precisely, binary variables, are often used to model purchase decisions. In our context i.e. to model the decision whether to employ a specific pump type within the system or not. Moreover, binary variables are used to model the activation or deactivation of active components, i.e. an on/off-switch.

Therefore, case (ii), integer variables being present in both stages, occurs when the model takes into account that not all pumps are always switched on to meet the demand of the different load scenarios. In contrast, some pumps may also be switched off and bypassed for efficiency reasons, especially in load cases with lower volume flow requirements.

Theoretical aspects of the problems of case (ii), also called complete mixed-integer recourse problems, have e.g. been investigated by Schultz [1992], and sophisticated solution approaches have been proposed, cf. e.g. Carøe and Tind [1998]. Resting on the formulation as deterministic equivalent program, standard solution approaches based on Branch & Bound with LP relaxation may be applied. Yet these might suffer from high computation times, especially if multiple (load) scenarios are considered in the second stage.

3. Technical Application

As mentioned in the previous sections, we generate models to compute energy-efficient centralized and decentralized booster stations in high-rise buildings and validate these models on a test rig. The physical properties of these systems and topology decisions are modeled within the constraints of the optimization programs. In this work the objective is to minimize the simplified life-time cost, which consist of investment and energy costs within the lifetime. These two parts represent the most important goals, cf. Tolvanen [2007], when designing pumping systems. When modeling these systems, two aspects are of importance. First, reasonable computation times of the model are required. Second, the model's level of detail has to represent the real system with an acceptable accuracy to allow for the transfer of the optimization results. The computed optimum within the model, should represent the true optimum of the underlying technical system. Usually, a trade-off between these two goals is necessary, as the former tends to lead to models that are as simple as possible, while the latter demands for models that are highly accurate, but computationally not tractable. To achieve a

model, that is as simple as possible and at the same time as accurate as needed, we conduct a validation step based on a test rig that represents a scaled building with five pressure zones. We present all relevant basics of the system modeling, the test rig and the used pumps in the following paragraphs.

3.1. **System Modeling.** The booster station can be modeled as a graph $\mathcal{G} = (\mathcal{V}, \mathcal{E})$, in which the edges $\mathcal{E}$ model the pumps as well as the pipes of the considered booster station. The junctions of the booster station are modeled as vertices $\mathcal{V}$. We distinguish three different booster station topologies, which differ in the alignment of the pumps. Today, pumps are commonly aligned in parallel at the lowest pressure zone of the building. This leads to a central, parallel booster station design providing the pressure and volume flow for the whole building. Varying from this approach, also the serial arrangement of pumps in a central booster station is possible, leading to higher degrees of freedom in the design process and therefore allowing for higher energy efficiency of the booster station. For the centralized topology the building's demand can be modeled as solely one sink with one available water source. Additionally to these centralized system topologies a decentralized booster station topology is possible. In this approach, pumps can be positioned at any pressure zone of the building and therefore a more accurate modeling of the volume flow demand is necessary. In this case each pressure zone can be modeled as an individual sink, which represents a different pressure zone in the building. The decentralized topology allows for an even higher degree of freedom to improve the overall efficiency even further.

The graph representation of an exemplified system is shown in Fig. 1. In this exemplary system three pumps are used. The first pump is used in series with the two other pumps. The second and third pump supply different pressure zones in the building individually. Within this contribution, the fresh cold water supply is considered solely, while waste water, hot water, and water for firefighting are not considered.

All pumps are modeled with polynomial approximations for the pressure volume flow characteristic, as well as the power volume flow characteristic. This approach is based on Ulanicki et al. [2008]. We model the pressure increase $\Delta p = f(q, n)$ with $f : \mathbb{R}_0^+ \times \mathbb{R}_0^+ \to \mathbb{R}_0^+$ by using a quadratic approximation relating the pressure head Δp, the volume flow $q \in \mathbb{R}_0^+$ and the normalized rotational speed $n \in [\underline{N}, \overline{N}]$, as given by

$$\Delta p = \sum_{m=0}^{2} \alpha_m \, q^{2-m} \, n^m, \tag{1}$$

where the parameters α_m and the lower bound of the normalized rotational speed $\underline{N}$ depend on the pump type. The rotational speed is normalized by using its maximum value. Therefore, we get an upper bound $\overline{N} = 1$. For better readability, we call the normalized rotational speed in the following only rotational speed or speed. The power $po = g(q, n)$ with $g : R_0^+ \times \mathbb{R}_0^+ \to$

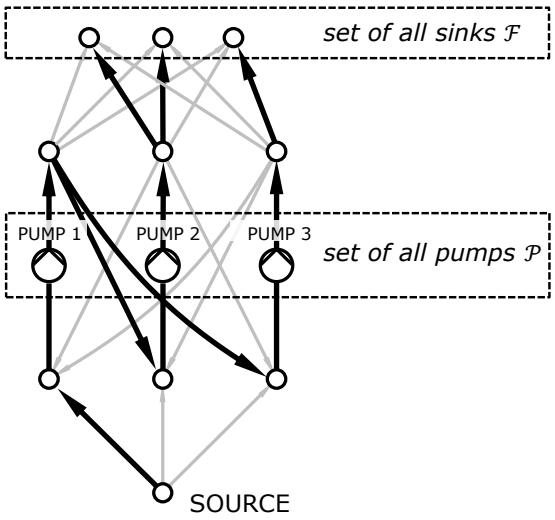

FIGURE 1. Graph representation of the underlying optimization program.

$\mathbb{R}_0^+$ is modeled by using a cubic approximation,

$$po = \sum_{m=0}^{3} \beta_m \, q^{3-m} \, n^m. \tag{2}$$

The parameters β_m in Eq. 2 are derived from manufacturer provided component characteristics for each pump type. Exemplified characteristic diagrams for a pump are shown in Fig. 2. The shown characteristics are often limited by maximum power as well as minimum and maximum volume flow requirements for each pump. These limits are added in the underlying optimization as additional constraints to model a realistic pump behavior. For simplicity they are not shown in Fig. 2.

The function of the booster station is to provide sufficient pressure to overcome the geodetic height and friction in the pipes. The required pressure is set together with the volume flow as a boundary condition at each sink node. When determining the demand, friction in the pipes is taken into account, as described later. Friction losses due to the connection of pumps within the booster station, e.g. due to elbow or tee fittings, are not considered, since it is of minor importance for real building. For the test rig, friction caused by the installation fittings of the pumps, e.g. to measure the pressure, is taken into account in the loss coefficient ζ_{inst}, cf. Sec. 7.

3.2. **Test Rig.** As described before, a validation of the optimization results is crucial to guarantee the technical functionality. A validation using real buildings is not possible for reasons of high effort. In addition, novel concepts shall be investigated, which cannot be realized on already existing buildings.

For this reason, a down-scaled, modular test rig has been set up, cf. Fig. 3 and Müller et al. [2019b]. The down-scaled system's booster station has the

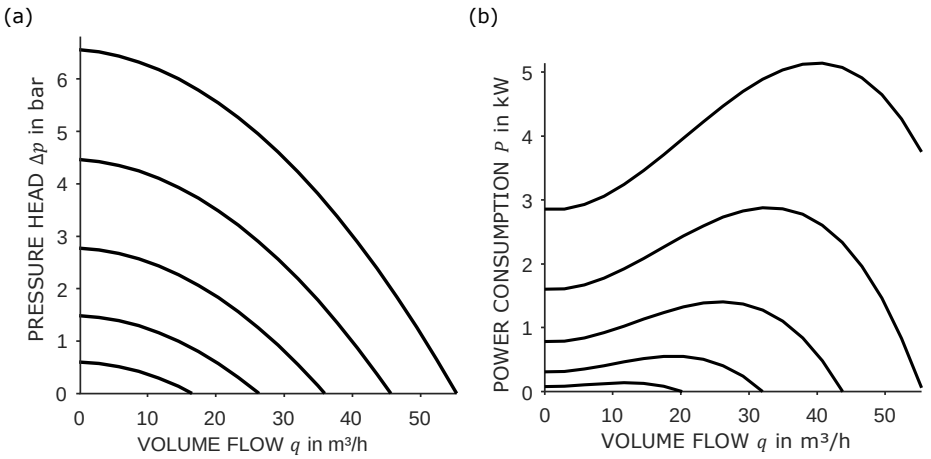

FIGURE 2. Exemplified characteristics for an example pump based on the used pump model. These characteristics are usually limited in each domain according to specific pump requirements. The different curves describe several different rotational speeds.

same characteristics as those of high-rise buildings. The geodetic height difference is 5 m and there are five different pressure zones, which can be supplied individually. The water is pumped from a tank with constant pressure to the five pressure zones by the booster station. As in real buildings, the water flows out at ambient pressure (open system) and returns to the tank through a drainpipe. The test rig is equipped with sensors for measuring the volume flow in each pressure zone as well as the pressure head and power consumption of each pump. It is possible to control the rotational speed of the pumps and the valve position on each pressure zone and thus to control the volume flow on each pressure zone. Overall, a set of thirteen different pumps, consisting of six different types, is available (cf. Fig. 5). The pumps are centrifugal circulator pumps for heating systems with an integrated frequency converter (FC) and therefore speed controllable. The size is chosen to fit the needs for the down-scaled booster system, even though the ratio of pressure head to volume flow is lower as for real world booster stations pumps. The pumps can be connected in any way and up to six pumps can be operated simultaneously as a booster station for the test rig.

3.3. **Load Scenarios.** We consider three different high-rise hotel buildings next to the previously described test rig as examples for the presented system optimization approach. The estimation of volume flow demands for these buildings is highly uncertain, if no usage patterns are known previously to the optimization. Therefore, it is always desired to use real data as input for the optimization method. An overview of water demand for hotel buildings is given by Gössling et al. [2012]. Besides these different measurements, Hirschberg [2014] also presented an approximation method to estimate the volume flow demand in buildings of different types. Another possibility to

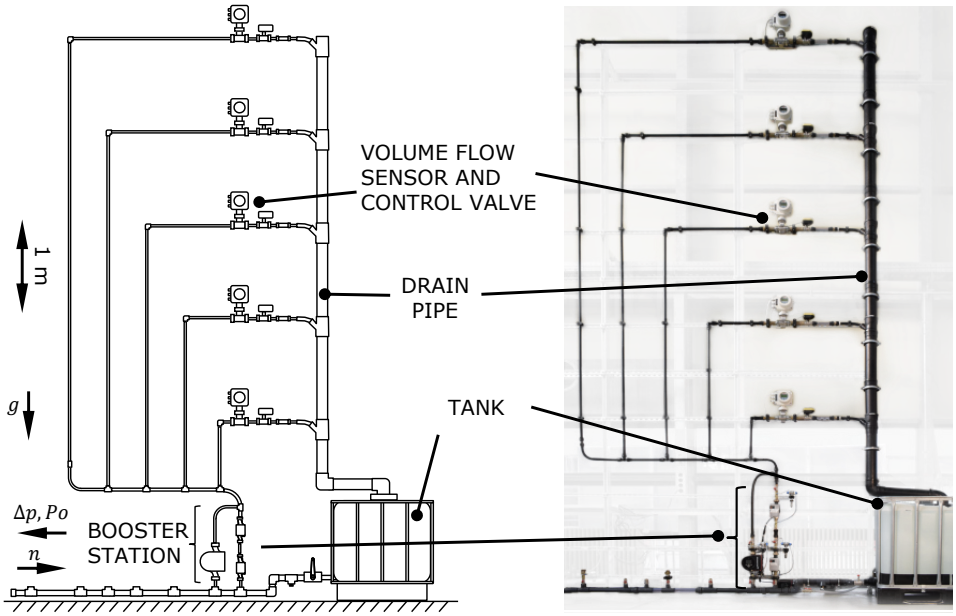

FIGURE 3. Sketch (left) and photo (right) of the modular test rig.

approximate the volume flow in buildings is given by DIN 1988-300. It shows a computational approach to estimate the volume flow demand in buildings based on a standardized estimation procedure.

The volume flow demand in building 3, as shown in Tab. 1, is based on current usage data in this building, while we use the estimation method shown by Hirschberg [2014] for building 1 and 2. The different buildings are referred to as B1, B2 and B3, respectively, when defining the instances for computation. The demand of the test rig system is derived by scaling the demands of real buildings according to the size of the test rig. We assume that all buildings in Tab. 1 are supplied by 5 pressure zones similarly to the test rig.

TABLE 1. Characteristics of the chosen example hotel buildings and the down-scaled test rig.

	unit	building 1	building 2	building 3	test rig
H	m	100	80	40	5
$\overline{Q}$	$m^3\,h^{-1}$	72	82	18	4.28
floors	–	28	23	10	–
pressure zones	–	5	5	5	5

The maximum load scenario – given by the maximum volume flow demand $\overline{Q}$ and maximum pressure head p_s – allows to lay out the booster station for the peak load. This load scenario occurs only for a fraction of the operation time. To design the booster station more realistically, we also consider the events of partial load. The volume flow demand in partial load is derived according to Hirschberg [2014] and all scenarios are shown in Fig. 4.

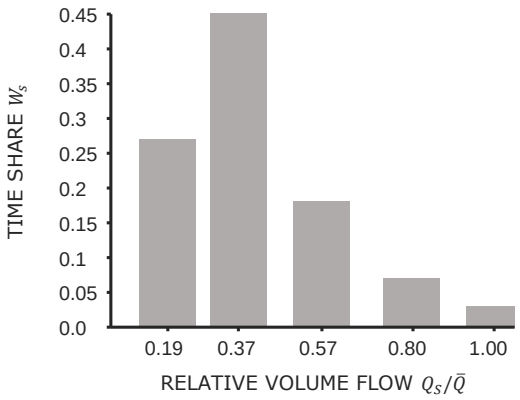

FIGURE 4. Load scenarios based on Hirschberg [2014] and the according time share.

The necessary pressure at the sink of a central booster station is calculated using the geodetic height of the building H, the minimum flow pressure $p_{\text{flow}} = 1\,\text{bar}$, the supply pressure $p_{\text{sup}} = 3\,\text{bar}$ and the friction, which depends quadratically on the flow rate. According to Hirschberg [2014], the pressure loss due to friction in the maximum load case is approximately $\sigma = 52\,\%$ of the geodetic and minimum flow pressure. This leads to:

$$\begin{aligned} p_s = \varrho g H + p_{\text{flow}} + \frac{1}{2}\varrho\zeta\left(\frac{Q_s}{A}\right)^2 - p_{\text{sup}} = \\ (\varrho g H + p_{\text{flow}})\left(1 + \sigma\left(\frac{Q_s}{\bar{Q}}\right)^2\right) - p_{\text{sup}} \quad \forall s \in \mathcal{S}. \end{aligned} \tag{3}$$

For the decentralized system design, we derive individual load scenarios for each pressure zone which sum up to the load scenarios in Fig. 4. The pressure at the different sinks is derived by scaling the pressure for the central booster station according to the geodetic height and the volume flow of the individual pressure zones.

3.4. **Selection of Pumps.** A crucial step in the design of booster stations for high-rise buildings is the selection of an appropriate set of available pumps, as shown by Leise and Altherr [2018]. We use a model series of 200 different market-available pumps which were explicitly designed for the water supply of buildings. As we also consider investment decisions within our optimization, we rely on market prices for the European Union of the year 2018. In our computations we consider different instances, e.g. differing in the type of building. As an optimization with all available 200 pumps is not feasible within reasonable computation time and most pumps are not suitable for each specific building, we reduce the number of considered pumps based on domain-specific knowledge. The set of pumps for the respective buildings are selected based on expert knowledge as for example shown by Larralde and Ocampo [2010a] and Larralde and Ocampo [2010b]. To the best of the authors knowledge there exists no general purpose method to

Algorithm 1: Heuristic Selection of Pumps

input : original load scenarios in Δp–q domain $\mathcal{S}$
set of all available pumps $\mathcal{P}^{\text{total}}$
distance parameter $d^{\max}$
set of desired fractional positions $\mathcal{F}$
output: selected pumps $\mathcal{P}$
$\mathcal{Z} \leftarrow \emptyset$ `// selected fractional loads in` Δp-q `domain`
$\mathcal{P} \leftarrow \emptyset$ `// selected pumps`
`// step 1: select fractional loads`
for $i \leftarrow 1$ **to** $|\mathcal{S}|$ **do**
  generate fractional loads for parallel pump usage based on $\mathcal{F}$ and add them to $\mathcal{Z}$
for $i \leftarrow 1$ **to** $|\mathcal{Z}|$ **do**
  generate fractional loads for serial pump usage based on $\mathcal{F}$ and add them to $\mathcal{Z}$
sort $\mathcal{Z}$ by power
while *true* **do**
  compute distance matrix $d_{i,j}$ between every point in $\mathcal{Z}$
  if *at least one* $d_{i,j} < d^{max} \forall\, i, j \in \mathcal{Z}$ *without* $i = j$ **then**
    remove point with $d_{i,j} < d^{\max}$ and lowest possible power from $\mathcal{Z}$
  else
    quit loop
`// step 2: get best suitable pumps for` $\mathcal{Z}$
for $i \leftarrow 1$ **to** $|\mathcal{Z}|$ **do**
  for $j \leftarrow 1$ **to** $|\mathcal{P}^{total}|$ **do**
    select best suitable pump $p_j \in \mathcal{P}^{\text{total}}$ for $z_i \in \mathcal{Z}$
    save best suitable pump in $\mathcal{P}$ if not already selected

select multiple appropriate pumps for high-rise buildings. Therefore, we use a selection heuristic, as shown in Alg. 1 for the pump selection, based on a two-step process.

In the first step, we define additional new load scenarios that should be met by individual pumps. These scenarios are derived from the original scenarios (Fig. 4): We allow for fulfilling the different load scenarios by individual groups of pumps, respectively. These pump groups consist of the same pump types, connected in parallel and/or serial. This results in a degradation of the original load scenarios to integral fractions of the original load scenarios, which are marked by gray circles in Fig. 5 for each building. The original load scenarios are represented by black square markers in Fig. 5. For each building we consider 15 different scenarios in the presented selection process for a pump construction kit accordingly consisting of 15 pumps in total. As the number of fractional loads results in a clustering of fractional load scenarios with small power, we use a set distance in the Δp–q domain to select only points which have a predefined distance from each other. We then iteratively delete load scenario points with a lower hydraulic power demand in the range of the set distance. With this reduction step, we assure, that every deleted load scenario point remains feasible in the solution, as we could use a pump with a higher hydraulic power and a frequency converter to reduce the rotational speed according to the desired fractional demand. Additionally it would be possible in a real building to throttle the flow to achieve the desired partial load scenario. This simple procedure ensures to derive the predefined number of pumps as well as a great coverage of the overall domain.

In the second step we select an appropriate pump for each of the remaining points in the Δp–q domain. A pump is selected, if it can fulfill

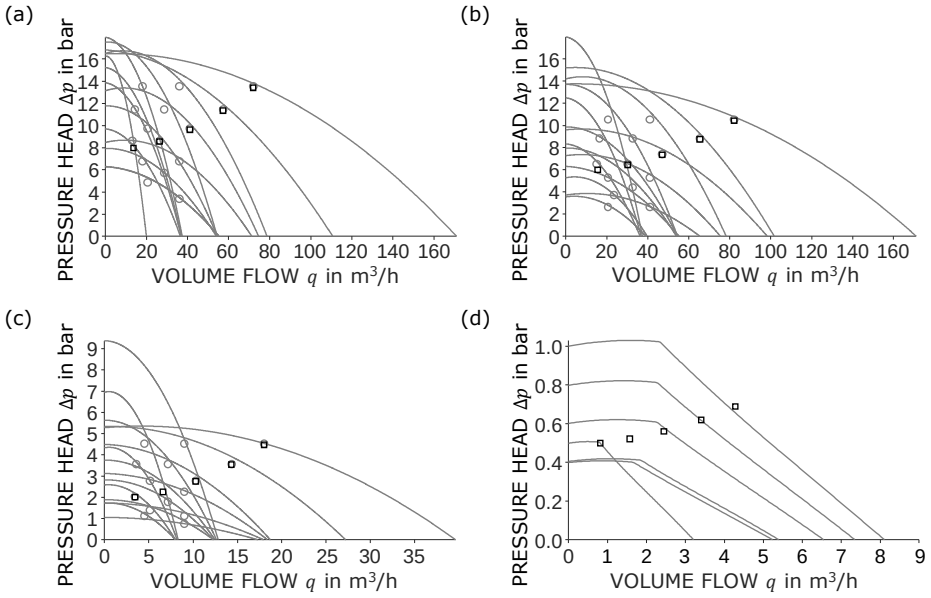

FIGURE 5. Characteristic diagrams of all used pumps at their maximum rotational speed for (a) building B1 of 100 m height, (b) building B2 of 80 m height, (c) building B3 of 40 m height, and (d) test rig . The considered scenarios are shown with black squares. The scaled points to select pumps in Alg. 1 are shown with gray circles for the three buildings.

the desired demand at these fractional loads and has the lowest possible maximum hydraulic power. In this manner we derive a final pump catalog that consists of a predefined number of pumps which are suitable to supply each original demand by single pumps or a combination of serial/parallel connected pumps. Additionally each selected pump has the lowest power demand to supply the partial load it was selected for. By implementing and applying this heuristic, we remove all pumps that are not suitable for the supply of a respective building, and therefore consider a predefined number of pumps that can supply the building efficiently.

4. Optimization Model

This section deals with the mathematical formulation of the previously introduced technical design problem. The technical specifications are modeled in a basic optimization model (Sec. 4.1) by constraints and the objective of overall minimal total cost. Since pumps have nonlinear characteristics, the Mixed-Integer Nonlinear Program (MINLP) pump model (Sec. 4.2) as well as two linear pump models, allowing the formulation of a Mixed-Integer Program (MIP), are presented. In a first approach, a piecewise linearized pump model (Sec. 4.3) is derived and in a second approach, a piecewise linear relaxed pump model (Sec. 4.4) is established.

TABLE 2. Decision Variables, Sets and Parameters.

Variable	Domain	Description
$\Delta p_{i,s}$; $q_{i,s}$; $n_{i,s}$	$\mathbb{R}_0^+$	Pressure increase, volume flow, rotational speed and power consumption of pump $i \in \mathcal{P}$ in scenario $s \in S$.
$po_{i,s}^{\text{pump}}$; $po_{i,s}^{\text{FC}}$; $po_{i,s}$	$\mathbb{R}_0^+$	Power consumption of pump $i \in \mathcal{P}$, the associated frequency converter and the sum of both in scenario $s \in S$.
$p_{i,s}^{\text{in}}$; $p_{i,s}^{\text{out}}$	$\mathbb{R}_0^+$	Pressure at inlet and outlet of pump $i \in \mathcal{P}$, $s \in \mathcal{S}$.
$q_{i,j,s}^{\text{pipe}}$	$\mathbb{R}_0^+$	Volume flow between outlet of pump i and inlet of pump j, $i, j \in \mathcal{P}$, $s \in \mathcal{S}$.
$q_{i,s}^{\text{source}}$	$\mathbb{R}_0^+$	Volume flow between source and inlet of pump $i \in \mathcal{P}$, $s \in \mathcal{S}$.
$q_{i,f,s}^{\text{sink}}$	$\mathbb{R}_0^+$	Volume flow between outlet of pump $i \in \mathcal{P}$ and sink $f \in \mathcal{F}$, $s \in \mathcal{S}$.
		Indicator for connection between:
$t_{i,j}$	$\{0,1\}$	outlet of pump i and inlet of pump j,
t_i^{source}	$\{0,1\}$	source and inlet of pump i,
$t_{i,f}^{\text{sink}}$	$\{0,1\}$	outlet of pump i and sink $f \in \mathcal{F}$.
$x_{i,s}$	$\{0,1\}$	Activation of pump i in scenario $s \in S$.
y_i; y_i^{FC}	$\{0,1\}$	Investment decision for pump $i \in \mathcal{P}$ and associated frequency converter.

Set	Description
$\mathcal{P}$	Set of available pumps.
$\mathcal{S}$	Set of demand scenarios with $\lvert\mathcal{S}\rvert = 5$.
$\mathcal{F}$	Set of sinks, which corresponds to individually supplied pressure zones. For central systems applies $\lvert\mathcal{F}\rvert = 1$, for decentral systems $\lvert\mathcal{F}\rvert = 5$.

Parameter	Range	Description
APF	$\mathbb{R}_0^+$	Annuity-present value factor.
$C_{\text{invest},i}^{\text{pump}}$	$\mathbb{R}_0^+$	Investment costs of pump $i \in \mathcal{P}$.
$C_{\text{invest},i}^{\text{FC}}$	$\mathbb{R}_0^+$	Investment costs of frequency converter for pump $i \in \mathcal{P}$.
C_{elect}	$\mathbb{R}_0^+$	Electricity price (0.3 €/kWh).
W_s	$[0,1]$	Time share of scenario $s \in \mathcal{S}$.
T_{on}	$\mathbb{R}_0^+$	Total runtime per year ($0.3 \times 365d \times 24h$).
N^{buy}	$\mathbb{N}$	Maximum number of pumps that can be purchased.
$\overline{\Delta P_i}$; $\overline{P}$; $\overline{Q}$; $\overline{Po_i}$; $\underline{Po_i}$; $\underline{N}_i$, $\overline{N}_i$	$\mathbb{R}_0^+$	Upper ¯ and lower _ bounds for the pumps' operating parameters, i.e., pressure increase, pressure, volume flow, power, speed.
P_s^{source}	$\mathbb{R}_0^+$	Pressure at the source.
$P_{f,s}^{\text{sink}}$; $Q_{f,s}^{\text{bound}}$	$\mathbb{R}_0^+$	Pressure and volume flow demand at sink $f \in \mathcal{F}$ in scenario $s \in \mathcal{S}$.
Po_s^{hydr}	$\mathbb{R}_0^+$	Required hydraulic power $s \in \mathcal{S}$.
$\alpha_{i,m}$	$\mathbb{R}_0^+$	Pressure-volume flow regression coefficients for pump $i \in \mathcal{P}$ with $m \in \{0,1,2\}$.
$\beta_{i,m}$	$\mathbb{R}_0^+$	Power-volume flow regression coefficients for pump $i \in \mathcal{P}$ with $m \in \{0,1,2,3\}$.
$\zeta^{\text{inst.}}$	$\mathbb{R}_0^+$	Loss coefficient for the installation fittings of the pumps.
$\eta_{\text{best}}^{\text{pump}}$	$\mathbb{R}_0^+$	Best efficiency of any pump in set $\mathcal{P}$.
η_i^{FC}	$\mathbb{R}_0^+$	Efficiency of frequency converter of pump $i \in \mathcal{P}$.

4.1. **Basic Optimization Model.** All derived optimization models in this contribution have a common mixed-integer linear foundation, which we present in this section. The basic model's variables, which are indicated by lower case letters, as well as sets and parameters, indicated by upper case and Greek letters, are shown in the Tab. 2.

The shared objective of all presented optimization models is the maximization of the net present value, cf. Meck et al. [2019]. This results in a minimization of lifetime cost, which are approximated considering investment costs for pumps and frequency converters as well as discounted energy costs. The objective is shown in Eq. (5a). We use the annuity-present value factor APF to discount all costs to the present day.

We model an upper bound of pumps, (5b), to solely select a suitable subset of all possible pumps in $\mathcal{P}$ in the final solution, i.e. maximum N^{buy} pumps may be bought. The necessary precondition to use a pump is that it was bought, (5c). Purchased pumps should be used only in their physical domain. Therefore, we limit the pump speed, power and volume flow with Constr. (5d) and (5e). Constr. (5f) models the volume flow conservation in the network, while Constr. (5g) models upper bounds for the volume flow in each pipe. We demand the volume flow in the sinks to be exactly the predefined volume flow for each scenario, as shown in Fig. 4 with Constr. (5h). It is imperative to choose at least one pump to connect the source with the sinks, (5i) and (5j). Constr. (5k)–(5m) prevent undesired topologies, as for example loops. The pressure at the inlet of a pump is set to the pressure at the source P_s^{source} in Constr. (5n) if a pump is connected to the source. The pressure increase from the inlet to the outlet of a pump is modeled by Constr. (5o). The pressure at the inlet and outlet of a not used pump is set to zero, Constr. (5p). The pressure of an pumps' outlet should fulfill the predefined pressure requirements at the sink if it is connected to the sink, (5q). The pressure propagation between connected pumps is modeled by Constr. (5r). If a frequency converter for a certain pump is not purchased ($y_i^{FC} = 0$), the speed of the pump has to be set to the nominal speed ($n = 1$) in case of activity, Constr. (5s). If the pump is turned off, or an frequency converter is purchased, this constraint has to be deactivated, Constr. (5s). If a frequency converter is bought the pump is speed controllable, but a part of the transmitted electrical power is dissipated, Constr. (5t). In addition, the electric power for the pump motor is added to the total power, Constr. (5u). The electrical power of the system has to be higher than the hydraulic power divided by the best efficiency of the best pump, Constr. (5v). This provides a lower bound for the power consumption, which significantly speeds up the optimization process, as shown by Müller et al. [2019a].

In the subsequently introduced models, we allow for the option to restrict the usage of in series connected pumps, as pumps connected in parallel correspond to the current standard installation procedure. A parallel connection can be achieved by adding the following constraint to the basic model (5):

$$t_{i,j} = 0 \quad \forall\, i, j \in \mathcal{P}. \tag{4}$$

All presented constraints, (5) and (4), depend linearly on the decision variables. This accordingly Mixed-Integer Program describes the generic selection and usage of pumps to supply multiple sinks with relevant connected pumps to derive a suitable booster station. Nevertheless, this model does not contain the explicit modeling of the used pumps, as shown in Eq. (1) and Eq. (2). Therefore, we present different methods to model these nonlinear relations of type $\Delta p = f(q, n)$ and $po = g(q, n)$ in the following subsections.

$$\min \quad T_{\text{on}} APF\, C_{\text{elect}} \sum_{s\in S} W_s \sum_{i\in\mathcal{P}} po_{i,s} + \sum_{i\in\mathcal{P}} C^{\text{pump}}_{\text{invest},i}\, y_i + \sum_{i\in\mathcal{P}} C^{\text{FC}}_{\text{invest},i}\, y^{\text{FC}}_i \tag{5a}$$

subject to

$$\sum_{i\in\mathcal{P}} y_i \le N^{\text{buy}} \tag{5b}$$

$$x_{i,s} \le y_i \quad \forall i\in\mathcal{P}, s\in\mathcal{S} \tag{5c}$$

$$n_{i,s} \ge \underline{N}_i x_{i,s} \quad \forall i\in\mathcal{P}, s\in\mathcal{S} \tag{5d}$$

$$\begin{aligned}\Delta p_{i,s} \le \overline{\Delta P_i} x_{i,s},\ q_{i,s} \le \overline{Q} x_{i,s},\ n_{i,s} \le \overline{N}_i x_{i,s},\\ po_{i,s} \le \overline{Po}_i,\ po^{\text{pump}}_{i,s} \le \overline{Po}_i x_{i,s} \quad \forall i\in\mathcal{P}, s\in\mathcal{S}\end{aligned} \tag{5e}$$

$$q_{i,s} = \sum_{j\in\mathcal{P}} q^{\text{pipe}}_{j,i,s} + q^{\text{source}}_{i,s} = \sum_{j\in\mathcal{P}} q^{\text{pipe}}_{i,j,s} + \sum_{f\in\mathcal{F}} q^{\text{sink}}_{i,f,s} \quad \forall i\in\mathcal{P}, s\in\mathcal{S} \tag{5f}$$

$$q^{\text{pipe}}_{i,j,s} \le \overline{Q} t_{i,j},\ q^{\text{source}}_{i,s} \le \overline{Q} t^{\text{source}}_i,\ q^{\text{sink}}_{i,f,s} \le \overline{Q} t^{\text{sink}}_{i,f} \quad \forall i,j\in\mathcal{P}, f\in\mathcal{F}, s\in\mathcal{S} \tag{5g}$$

$$\sum_{i\in\mathcal{P}} q^{\text{sink}}_{i,f,s} = Q^{\text{bound}}_{f,s} \quad \forall f\in\mathcal{F}, s\in\mathcal{S} \tag{5h}$$

$$\sum_{i\in\mathcal{P}} t^{\text{sink}}_{i,f} \ge 1 \quad \forall f\in\mathcal{F} \tag{5i}$$

$$\sum_{i\in\mathcal{P}} t^{\text{source}}_i \ge 1 \tag{5j}$$

$$t_{i,i} = 0 \quad \forall i\in\mathcal{P} \tag{5k}$$

$$\sum_{j\in\mathcal{P}} t_{i,j} \le |\mathcal{P}|(1 - t^{\text{source}}_i) \quad \forall i\in\mathcal{P} \tag{5l}$$

$$\sum_{j\in\mathcal{P}} t_{i,j} \le |\mathcal{P}| y_i, \sum_{j\in\mathcal{P}} t_{j,i} \le |\mathcal{P}| y_i, t^{\text{source}}_i \le y_i, \sum_{t\in\mathcal{F}} t^{\text{sink}}_{i,f} \le y_i \quad \forall i\in\mathcal{P} \tag{5m}$$

$$p^{\text{in}}_{i,s} - P^{\text{source}}_s \overset{\le+}{\ge-} \overline{P}(1 - t^{\text{source}}_i) \quad \forall i\in\mathcal{P}, s\in\mathcal{S} \tag{5n}$$

$$p^{\text{in}}_{i,s} + \Delta p_{i,s} - p^{\text{out}}_{i,s} \overset{\le+}{\ge-} \overline{P}(1 - x_{i,s}) \quad \forall i\in\mathcal{P}, s\in\mathcal{S} \tag{5o}$$

$$p^{\text{in}}_{i,s} \le \overline{P}\left(\sum_{j\in\mathcal{P}} t_{j,i} + t^{\text{source}}_i\right), p^{\text{out}}_{i,s} \le \overline{P}\left(\sum_{j\in\mathcal{P}} t_{i,j} + \sum_{f\in\mathcal{F}} t^{\text{sink}}_{i,f}\right) \quad \forall i\in\mathcal{P}, s\in\mathcal{S} \tag{5p}$$

$$p^{\text{out}}_{i,s} - P^{\text{sink}}_{f,s} \overset{\le+}{\ge-} \overline{P}(1 - t^{\text{sink}}_{i,f}) \quad \forall i\in\mathcal{P}, f\in\mathcal{F}, s\in\mathcal{S} \tag{5q}$$

$$p^{\text{out}}_{i,s} - p^{\text{in}}_{j,s} \overset{\le+}{\ge-} \overline{P}(1 - t_{i,j}) \quad \forall i,j\in\mathcal{P}, s\in\mathcal{S} \tag{5r}$$

$$n_{i,s} - 1 \overset{\le+}{\ge-} \left((1 - x_{i,s}) + y^{FC}_i\right) \quad \forall i\in\mathcal{P}, s\in\mathcal{S}, \tag{5s}$$

$$\left(1 - \eta^{\text{FC}}_i\right) po_{i,s} - po^{\text{FC}}_{i,s} \le \overline{Po}_i \left(1 - y^{\text{FC}}_i\right) \quad \forall i\in\mathcal{P}, s\in\mathcal{S} \tag{5t}$$

$$po_{i,s} = po^{\text{pump}}_{i,s} + po^{\text{FC}}_{i,s} \quad \forall i\in\mathcal{P}, s\in\mathcal{S} \tag{5u}$$

$$\sum_{i\in\mathcal{P}} po_{i,s} \ge Po^{\text{hydr}}_s / \eta^{\text{pump}}_{\text{best}} \quad \forall s\in\mathcal{S} \tag{5v}$$

4.2. **Mixed-Integer Nonlinear Pump Model.** The most accurate modeling approach is a nonlinear approach, in which each considered pump is modeled with nonlinear constraints according to Eq. (1) and Eq. (2). We add all pumps by adding

$$\Delta p_{i,s} = (\alpha_{i,0} - \zeta^{\text{inst.}})\, {q_{i,s}}^2 + \sum_{m=0}^{2} \alpha_{i,m}\, {q_{i,s}}^{2-m}\, {n_{i,s}}^m \quad \forall i\in\mathcal{P}, s\in\mathcal{S}, \tag{6a}$$

$$po^{\text{pump}}_{i,s} = \sum_{m=0}^{3} \beta_{i,m}\, {q_{i,s}}^{3-m}\, {n_{i,s}}^m \quad \forall i\in\mathcal{P}, s\in\mathcal{S}, \tag{6b}$$

to the basic model in Eq. (5), where $\zeta^{\text{inst.}}$ is the pressure loss factor of the fittings used for installing the pump into the system. The benefits of this approach are a fast and highly accurate modeling, while the drawbacks are potentially high solution times.

4.3. **Piecewise Linearized Pump Model.** A common approach to solve nonlinear non-convex optimization models with integer variables, is to make use of approximations based on piecewise linearization (PWL) techniques, cf. Geißler et al. [2012]. Linearization of all nonlinear constraints results in a Mixed-Integer Program, which can then be solved by state-of-the-art solvers as for example GUROBI or CPLEX. Piecewise linearization methods are therefore applied in a high variety of applications, both within classical operations research, as well as technical applications, e.g. Mikolajková et al. [2018], Misener et al. [2009] and Morsi et al. [2012]. The underlying modeling to reformulate a nonlinear functional relationship as linear constraints can be implemented by multiple methods, as shown by Vielma et al. [2010], Geißler et al. [2012] and Misener and Floudas [2010].

In this contribution, we use the convex combination method, as described by Vielma et al. [2010], to model the nonlinear relations of the pressure head $\Delta p = f(q, n)$ and of the power $po = g(q, n)$ as piecewise linearized function approximations. All additional variables, sets and parameters for the PWL are shown in Tab. 3. Instead of using Eq. (6) to model the nonlinear pump characteristics, we model a piecewise linearized approximation by using the set of constraints (7).

TABLE 3. Additional Variables, Sets and Parameters for PWL.

Variable	Domain	Description
$\lambda_{u,v,i,s}$	$[0,1]$	Additional variable to model the piecewise linear approximation based on grid point (u,v) and pump $i \in \mathcal{P}$ in scenario $s \in S$.
$a_{i,s,k}$	$\{0,1\}$	Binary variable to select simplex $k \in \mathcal{K}$ for pump $i \in \mathcal{P}$ in scenario $s \in S$.
Set		**Description**
$\mathcal{Q}$		Set of grid points in q direction.
$\mathcal{N}$		Set of grid points in n direction.
$\mathcal{K}$		Set of simplices.
$\mathcal{K}(u,v,i,s)$		Subset of simplices, which contain grid point (u,v) for pump $i \in \mathcal{P}$ in scenario $s \in S$.
Parameter	**Range**	**Description**
$Q_{u,v,i}$		Grid values in q direction for pump $i \in \mathcal{P}$.
$N_{u,v,i}$		Grid values in n direction for pump $i \in \mathcal{P}$.
$\Delta P_{u,v,i}$		Pressure value at grid point $(Q_{u,v,i}, N_{u,v,i})$ by evaluating Eq. 1 for pump $i \in \mathcal{P}$.
$Po_{u,v,i}$		Power value at grid point $(Q_{u,v,i}, N_{u,v,i})$ by evaluating Eq. 2 for pump $i \in \mathcal{P}$.

$$q_{i,s} - \sum_{u\in\mathcal{Q}}\sum_{v\in\mathcal{N}} \lambda_{u,v,i,s} Q_{u,v,i} \overset{\leq+}{\geq-} (1-x_{i,s})\overline{Q} \quad \forall i \in \mathcal{P}, s \in \mathcal{S}, \tag{7a}$$

$$n_{i,s} - \sum_{u\in\mathcal{Q}}\sum_{v\in\mathcal{N}} \lambda_{u,v,i,s} N_{u,v,i} \overset{\leq+}{\geq-} (1-x_{i,s}) \quad \forall i \in \mathcal{P}, s \in \mathcal{S}, \tag{7b}$$

$$\Delta p_{i,s} - \sum_{u\in\mathcal{Q}}\sum_{v\in\mathcal{N}} \lambda_{u,v,i,s} \Delta P_{u,v,i} \overset{\leq+}{\geq-} (1-x_{i,s})\overline{\Delta P_i} \quad \forall i \in \mathcal{P}, s \in \mathcal{S}, \tag{7c}$$

$$po_{i,s}^{\text{pump}} - \sum_{u\in\mathcal{Q}}\sum_{v\in\mathcal{N}} \lambda_{u,v,i,s} Po_{u,v,i}^{\text{pump}} \overset{\leq+}{\geq-} (1-x_{i,s})\overline{Po_i} \quad \forall i \in \mathcal{P}, s \in \mathcal{S}, \tag{7d}$$

$$\sum_{u\in\mathcal{Q}}\sum_{v\in\mathcal{N}} \lambda_{u,v,i,s} = 1 \quad \forall i \in \mathcal{P}, s \in \mathcal{S}, \tag{7e}$$

$$\sum_{k\in\mathcal{K}} a_{i,s,k} = 1 \quad \forall i \in \mathcal{P}, s \in \mathcal{S}, \tag{7f}$$

$$\lambda_{u,v,i,s} - \sum_{k\in\mathcal{K}(u,v,i,s)} a_{i,s,k} \leq 0 \quad \forall u \in \mathcal{Q}, v \in \mathcal{N}, i \in \mathcal{P}, s \in \mathcal{S}. \tag{7g}$$

The index sets $\mathcal{Q}$ and $\mathcal{N}$ represent grid points in the (q, n) domain in which the pressure $\Delta P_{u,v,i,s}$ and power $Po_{u,v,i,s}^{\text{pump}}$ are evaluated for each pump $i \in \mathcal{P}$ before optimization according to Eq. (1) and Eq. (2). The pressure losses and additional power for frequency converters are added to these values in the preprocessing of the optimization to derive an equivalent description, as shown in Constr. (6). Besides these grid points, we have to use additional binary variables $a_{i,s,k} \in \{0,1\}$ and continuous variables $\lambda_{u,v,i,s} \in [0,1]$ to ensure a piecewise linearized approximation. The set $\mathcal{K}$ in Constr. (7f) contains all segments of the piecewise linearized approximation. In turn, the subset $\mathcal{K}(u,v,i,s)$ in Constr. (7g) covers all segments that contain the grid point (u,v) for pump i and scenario s. These additional constraints are added to the optimization program in model (5), which results in a Mixed-Integer Linear Program that can be solved by common MIP solvers.

4.4. **Piecewise Linear Relaxed Pump Model.** As a third possibility we use piecewise linear relaxed pump models within the final optimization program. Relaxations are often used in the MINLP solution process, as shown by Puranik and Sahinidis [2017], to derive valid lower bounds. A general introduction to relaxation methods for nonlinear network design problems is given by Humpola and Fügenschuh [2015]. Relaxation methods with piecewise linear underestimators are also used in MINLP solvers to improve the solution speed, cf. Misener and Floudas [2012, 2013, 2014]. Besides these multi-purpose implementations these methods can also be used to improve the solution process for domain specific optimization models, like for example shown by Pecci et al. [2019] in the domain of water supply networks. The authors derived global bounds on the placement of valves, by using a Branch-and-Bound algorithm with relaxed nonlinear constraints. As shown in all previous references, the usage of piecewise relaxed underestimators can improve the solution process. For this reason, we developed a relaxed pump model to improve the solution speed of Alg. 2 in the following Sec. 5.

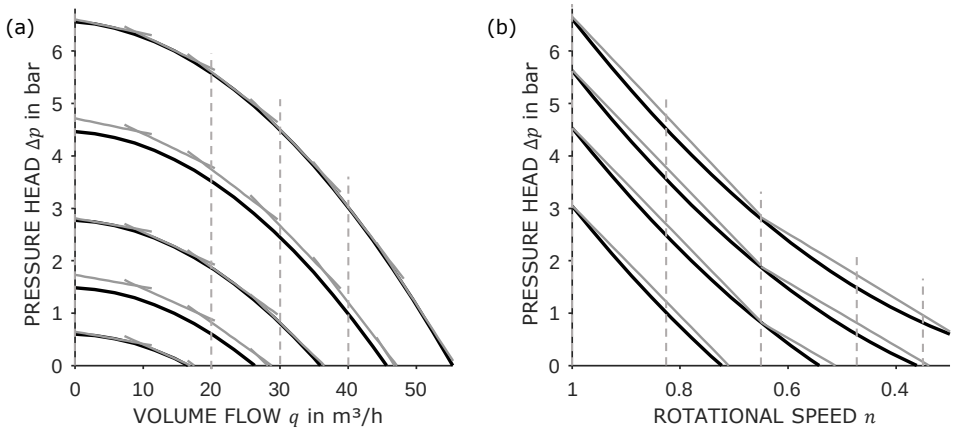

FIGURE 6. Piecewise linear overestimation of the quadratic function of the pressure $\Delta p = f(q, n)$. Shown are (a) the function $\Delta p(q)$ for different speeds n and (b) the function $\Delta p(n)$ for different volume flows q. $R = 6$ elements in q direction and $K = 2$ elements in n direction are used. The dashed lines in (a) show the values of q for which the lines were plotted in (b) and vice versa.

In order to underestimate the total cost it is necessary to overestimate the pressure increase and to underestimate the power consumption of the pumps:

$$\Delta p_{i,s} \leq \Delta p_{i,s}^{\text{relaxed}} \quad \forall i \in \mathcal{P}, s \in \mathcal{S}, \tag{8a}$$

$$po_{i,s}^{\text{pump}} \geq po_{i,s}^{\text{relaxed}} \quad \forall i \in \mathcal{P}, s \in \mathcal{S}. \tag{8b}$$

For these estimations, piecewise defined planes are used, which serve as linear under- or overestimators. They have to be defined piecewise, since $\Delta p = f(q, n)$ is not concave in n and $po^{\text{pump}} = g(q, n)$ is not convex in q. The functions are shown in Fig. 6 and Fig. 7 along with the over- and underestimations.

We define R equidistant segments in q and K equidistant segments in n direction. The boundaries of these segments are described by the sets $\mathcal{Q}^{\text{seg}} = \{Q_1^{\text{seg}}, ..., Q_{1+R}^{\text{seg}}\}$ and $\mathcal{N}^{\text{seg}} = \{N_1^{\text{seg}}, ..., N_{1+K}^{\text{seg}}\}$. For each segment (u, v) and each function ($\Delta p = f(q, n)$, $po^{\text{pump}} = g(q, n)$) a plane is defined, which should approximate the function as good as possible. Each plane is defined by the parameters $\gamma_{i,k,u,v}$ ($\Delta p = f(q, n)$) and $\delta_{i,k,u,v}$ ($po^{\text{pump}} = g(q, n)$) with $i \in \mathcal{P}$, $k \in \{1, 2, 3\}$, $u \in \{1, ..., R\}$, $v \in \{1, ..., K\}$.

To solve the overall MINLP, cf. Sec. 4, the constraints of the pump characteristics (6) are replaced by the following constraints:

Constraints (9a) and (9b) guarantee that the pressure in each segment is underestimated and the power overestimated. Here, $x_{i,s,v}^{\gamma}$ and $x_{i,s,u}^{\delta}$ are binary activation variables which activate a plane if and only if the speed (in case of pressure overestimation) or volume flow (in case of power underestimation) is within the segment boundaries. $\varepsilon = 10^{-3}$ is necessary to ensures that at least one plane is active at the boundaries of the piecewise

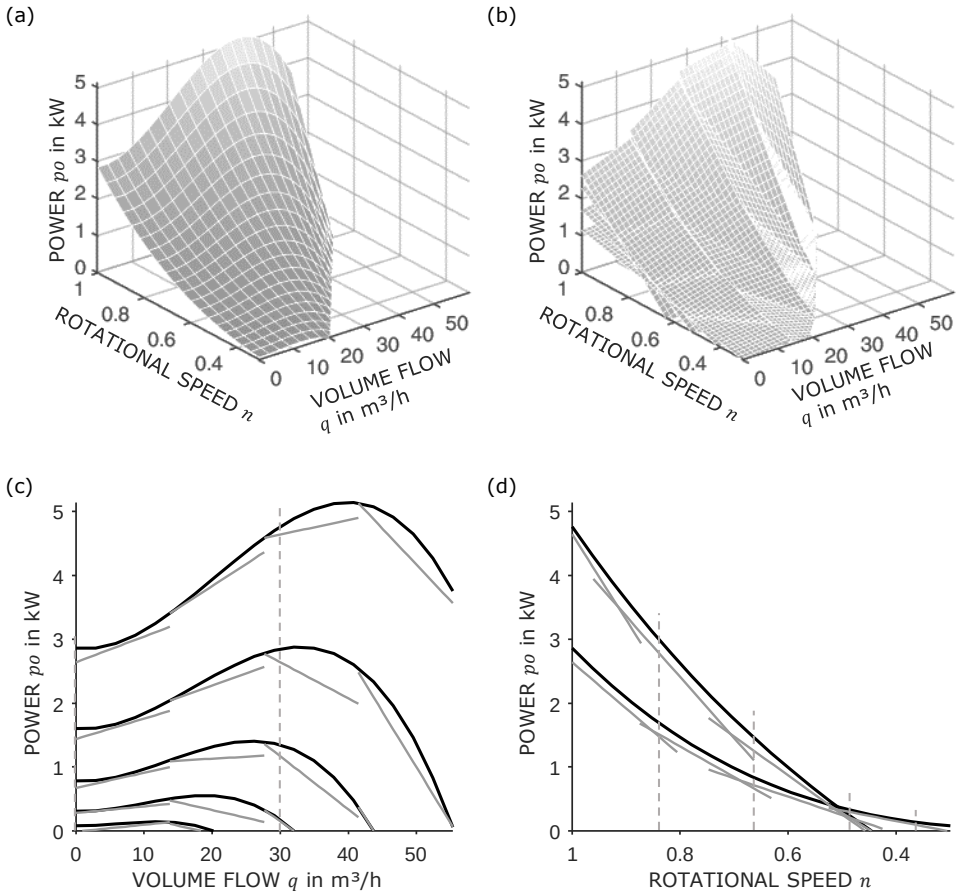

FIGURE 7. Piecewise linear underestimation of the cubic function of the power consumption $po = g(q, n)$. (a) shows the nonlinear function and (b) the piecewise underestimation. (c) shows the function $po(q)$ for different speeds n and (d) the function $po(n)$ for different volume flows (q). $R = 4$ elements in q direction and $K = 4$ elements in n direction are used. The dashed lines in (c) show the values of q for which the lines were plotted in (d) and vice versa.

defined planes. $\overline{M}_1$ and $\overline{M}_2$ are upper bounds which are necessary for the bigM-constraints. Constraints (9c) to (9h) are used to check the mentioned boundaries, with binary auxiliary variables $x^{\gamma 1}$, $x^{\gamma 2}$, $x^{\delta 1}$ and $x^{\delta 2}$.

The parameters of the planes are determined using a MIP. The objective is to find planes within a segment which describe the function as good as possible and over- or underestimate it. To model this, a fine grid $\mathcal{Q}^{\text{grid}}$ and $\mathcal{N}^{\text{grid}}$ is defined: at each grid point it is constrained that the overestimation or underestimation is maintained and the distance to the nonlinear function is calculated. The set $\mathcal{Q}^u$ with $u \in \{1, ..., R\}$ and $\mathcal{N}^v$ with $v \in \{1, ..., K\}$

$$\Delta p_{i,s} - (\gamma_{i,1,u,v}\, q_{i,s} + \gamma_{i,2,u,v}\, n_{i,s} + \gamma_{i,3,u,v}) \leq (1 - x^{\gamma}_{i,s,v})\overline{M}_1 \quad \forall u \in \{1,...,R\}, v \in \{1,...,K\}, i \in \mathcal{P}, s \in \mathcal{S} \tag{9a}$$

$$po^{\text{pump}}_{i,s} - (\delta_{i,1,u,v}\, q_{i,s} + \delta_{i,2,u,v}\, n_{i,s} + \delta_{i,3,u,v}) \geq -(1 - x^{\delta}_{i,s,u})\overline{M}_2 \quad \forall u \in \{1,...,R\}, v \in \{1,...,K\}, i \in \mathcal{P}, s \in \mathcal{S} \tag{9b}$$

$$x^{\gamma 1}_{i,s,v} + x^{\gamma 2}_{i,s,v} \leq x^{\gamma}_{i,s,v} \quad \forall v \in \{1,...,K\}, i \in \mathcal{P}, s \in \mathcal{S} \tag{9c}$$

$$n_{i,s} \geq (\mathcal{N}^{\text{seg}}_{v} + \varepsilon)(1 - x^{\gamma 1}_{i,s,v}) \quad \forall v \in \{1,...,K\}, i \in \mathcal{P}, s \in \mathcal{S} \tag{9d}$$

$$n_{i,s} - (\mathcal{N}^{\text{seg}}_{v+1} - \varepsilon) \leq (1 - x^{\gamma 2}_{i,s,v}) \quad \forall v \in \{1,...,K\}, i \in \mathcal{P}, s \in \mathcal{S} \tag{9e}$$

$$x^{\delta 1}_{i,s,u} + x^{\delta 2}_{i,s,u} \leq x^{\delta}_{i,s,u} \quad \forall u \in \{1,...,R\}, i \in \mathcal{P}, s \in \mathcal{S} \tag{9f}$$

$$q_{i,s} \geq (\mathcal{Q}^{\text{seg}}_{u} + \varepsilon)(1 - x^{\delta 1}_{i,s,u}) \quad \forall u \in \{1,...,R\}, i \in \mathcal{P}, s \in \mathcal{S} \tag{9g}$$

$$q_{i,s} - (\mathcal{Q}^{\text{seg}}_{u+1} - \varepsilon) \leq \overline{Q}(1 - x^{\delta 2}_{i,s,u}) \quad \forall u \in \{1,...,R\}, i \in \mathcal{P}, s \in \mathcal{S} \tag{9h}$$

describes the grid points within a segment. The following applies:

$$\mathcal{Q}^{u} = \{z \in \mathcal{Q}^{\text{grid}} | Q^{\text{seg}}_{u} \leq z \leq Q^{\text{seg}}_{u+1}\} \quad \forall u \in \{1,...,R\}, \tag{10a}$$

$$\mathcal{N}^{v} = \{z \in \mathcal{N}^{\text{grid}} | N^{\text{seg}}_{v} \leq z \leq N^{\text{seg}}_{v+1}\} \quad \forall v \in \{1,...,K\}. \tag{10b}$$

With these definitions MIP (11) for the pressure characteristic and MIP (12) for the power characteristics are formulated for each pump $i \in \mathcal{P}$ and for each segment (u, v) with $u \in \{1,...,R\}, v \in \{1,...,K\}$.

The objective (11a)/(12a) is to minimize the distance. Constraint (11b) models the overestimation of the pressure characteristic and Constr. (12b) the underestimation of the power characteristic at every grid point. Since the number of grid points is limited, distance factors $\varepsilon^{\Delta p} \in \mathbb{R}$ and $\varepsilon^{Po} \in \mathbb{R}$ are introduced to ensure that the planes are over/underestimating also between grid points. The result for the pressure characteristic is shown in Fig. 6 and for the power characteristic in Fig. 7.

$$\min \sum_{x=1}^{|\mathcal{Q}^u|} \sum_{y=1}^{|\mathcal{N}^v|} \left(\gamma_{i,1,u,v} Q^{\text{u}}_{x} + \gamma_{i,2,u,v} N^{\text{v}}_{y} + \gamma_{i,3,u,v}\right) - \left((\alpha_{i,0} - \zeta^{\text{inst.}})\,(Q^{\text{u}}_{x})^2 + \sum_{m=0}^{2} \alpha_{i,m}\,(Q^{\text{u}}_{x})^{2-m}\,(N^{\text{v}}_{y})^{m}\right) \tag{11a}$$

subject to

$$\gamma_{i,1,u,v} Q^{\text{u}}_{x} + \gamma_{i,2,u,v} N^{\text{v}}_{y} + \gamma_{i,3,u,v} \geq (\alpha_{i,0} - \zeta^{\text{inst.}})\,(Q^{\text{u}}_{x})^2 + \sum_{m=0}^{2} \alpha_{i,m}\,(Q^{\text{u}}_{x})^{2-m}\,(N^{\text{v}}_{y})^{m} + \varepsilon^{\Delta p} \quad \forall x \in \{1,...,|\mathcal{Q}^{\text{grid}}|\}, y \in \{1,...,|\mathcal{Q}^{\text{u}}|\} \tag{11b}$$

$$\min \sum_{x=1}^{|\mathcal{Q}^u|} \sum_{y=1}^{|\mathcal{N}^v|} \left(\beta_{i,1}(Q_x^{\mathrm{u}})^3 + \beta_{i,2}(Q_x^{\mathrm{u}})^2 N_y^{\mathrm{v}} + \beta_{i,3} Q_x^{\mathrm{u}}(N_y^{\mathrm{v}})^2 + \beta_{i,4}(N_y^{\mathrm{v}})^3 + \beta_{i,5}\right) - \left(\delta_{i,1,u,v} Q_x^{\mathrm{u}} + \delta_{i,2,u,v} N_y^{\mathrm{v}} + \delta_{i,3,u,v}\right) \tag{12a}$$

subject to

$$\begin{aligned} \beta_{i,1}(Q_x^{\mathrm{u}})^3 + \beta_{i,2}(Q_x^{\mathrm{u}})^2 N_y^{\mathrm{v}} + \beta_{i,3} Q_x^{\mathrm{u}}(N_y^{\mathrm{v}})^2 + \beta_{i,4}(N_y^{\mathrm{v}})^3 + \beta_{i,5} \geq \\ \delta_{i,1,u,v} Q_x^{\mathrm{u}} + \delta_{i,2,u,v} N_y^{\mathrm{v}} + \delta_{i,3,u,v} + \varepsilon^{\mathrm{Po}} \\ \forall x \in \{1, ..., |\mathcal{Q}^{\mathrm{grid}}|\}, y \in \{1, ..., |\mathcal{Q}^{\mathrm{u}}|\} \end{aligned} \tag{12b}$$

5. Solving Algorithm

The MINLP or piecewise linearized MIP presented in Sec. 4 can be solved with conventional solvers. This, however, leads to high computation times or large duality gaps for practically relevant problem sizes. For this reason, we developed a problem specific, exact solution algorithm, which allows significantly shorter computation times and leads to an acceptable result accuracy, even for the considered nonconvex MINLP.

The basic idea is to divide the problem into a number of smaller problems and to explore this solution space systematically. For this purpose, the set of all pumps $\mathcal{P}$ is reduced to a significantly smaller subset $\mathcal{P}^{\mathrm{reduced}} \subseteq \mathcal{P}$ and the purchase decisions for these pumps are fixed to one. This results in a fixation of the most important first stage decision variables. The number of pumps in the reduced set $|\mathcal{P}^{\mathrm{reduced}}|$ is less than or equal to the maximum number of pumps that can be purchased N^{buy}, which drastically reduces the number of binary variables: $|\mathcal{P}^{\mathrm{reduced}}| \leq N^{\mathrm{buy}} \ll |\mathcal{P}|$. If M is the number of different pump types in $\mathcal{P}$, then we can calculate the total number of tuples $I = |\mathcal{T}|$ with:

$$I = \binom{M + N^{\mathrm{buy}}}{M + 1} = \frac{(M + N^{\mathrm{buy}})!}{(M+1)! \cdot (N^{\mathrm{buy}} - 1)!}\,. \tag{13}$$

For the investigated instances ($M = 15$ and $N^{\mathrm{buy}} = 4$) this results in $I = 3876$ reduced MINLP with $|\mathcal{P}^{\mathrm{reduced}}| \leq 4$. When considering a decentral topology (e.g. test instance B1.D, cf. 6.1) this yields a MINLP with 425 variables (64 binary) and 1057 constraints (41 nonlinear). In contrast to this is a single MINLP with $|\mathcal{P}| = M \times N^{\mathrm{buy}} = 60$ pumps. This yields 26581 variables (4380 binary) and 82562 constraints (601 nonlinear). The resulting reduced MINLP is therefore less challenging in terms of combinatorics and can generally be solved faster. The goal is to efficiently explore the set of possible purchase decisions $\mathcal{T}$, given the reduced set of available pumps, while also cutting off non-optimal solutions.

The algorithm is shown in Alg. 2. For better clarity, we define the index set $\mathcal{I} = \{1, 2, \ldots, I\}$ based on Eq. (13). First, the set of pump-tuples $\mathcal{T}$ is created and physically inadmissible tuples are removed during preprocessing. In addition, a set of lower bounds $\mathcal{L} = \{L_1, L_2, \ldots, L_I\}$

Algorithm 2: Generic description of the solution algorithm.

input : set of pumps $\mathcal{P}$; load scenarios; instance-specific parameters
output: best topology and control; solution information

`// preprocessing`
initialize all possible feasible purchase decisions $\mathcal{T}$
$\mathcal{I} = \{1, 2, \ldots, I\}$
$\mathcal{L} = \{L_1, L_2, \ldots, L_I\}$
$\mathcal{U} = \{U_1, U_2, \ldots, U_I\}$
$\mathcal{U} \leftarrow U_j = \infty \, \forall \, j \in \mathcal{I}$
$\mathcal{L} \leftarrow L_j = \sum_{s \in S} W_s Po_s^{\text{hydr}} \, \forall \, j \in \mathcal{I}$
$U^{\text{global}} = \infty$, $L^{\text{global}} = \min(\mathcal{L})$

`// main part`
while $U^{\text{global}} > \mathcal{L}^{\text{global}}$ **do**

`// heuristic for upper-bound-search`
estimate primal bound for each tuple, $U_j^{\text{est}} \, \forall \, j \in \mathcal{I}$
solve reduced MINLP for the most promising tuple (lowest U_j^{est})
if *infeasible or dual bound* $> U^{\text{global}}$ **then**
  remove tuple
else
  update tuple information in: $\mathcal{U}, \mathcal{L}$
update global information: $U^{\text{global}} = \min(\mathcal{U}), L^{\text{global}} = \min(\mathcal{L})$

`// lower-bound-search`
solve reduced MINLP or relaxed, reduced MIP for tuple with lowest dual bound in $\mathcal{L}$
if *infeasible or dual bound* $> U^{\text{global}}$ **then**
  remove tuple
else
  update tuple information in: $\mathcal{U}$ (only if MINLP was solved), $\mathcal{L}$
update global information: $U^{\text{global}} = \min(\mathcal{U}), L^{\text{global}} = \min(\mathcal{L})$

for the energy costs of each tuple $T_j \in \mathcal{T}$ is analytically calculated based on domain-specific knowledge. Additionally, a set of all primal bounds $\mathcal{U} = \{U_1, U_2, \ldots, U_I\}$ is defined and each member is set to ∞ before optimization. For the considered overall minimization problem, the primal bound is the minimal primal solution of a tuple $U^{\text{global}} = \min(\mathcal{U})$ (best found solution), which is infinite at the start. The dual bound of the overall minimization problem L^{global} should be raised. This is determined by the weakest dual bound in one of the subproblems/tuples. Thus, the dual bound of the overall problem is bounded by the lowest dual bound of a tuple $L^{\text{global}} \geq \min(\mathcal{L})$. It is initialized using the preprocessed bounds for the energy and the known investment cost of the pumps. Now the search for better primal and dual solutions is repeated until the overall problem has been solved to proven global optimality. The global primal and dual bounds are updated in each step and proven weak solutions or infeasible solutions are cut off. In the following, the single steps of the algorithm are explained in detail.

5.1. **Preprocessing.** First, the set of purchase decisions $T_j \in \mathcal{T} \quad \forall j \in \mathcal{I}$, each consisting of a reduced set of pumps $\mathcal{P}_j^{\text{reduced}} \subseteq \mathcal{P}$ with $j \in \mathcal{I}$, is generated. For each tuple $T_j \in \mathcal{T}$, it is determined whether the pumps of the tuple $\mathcal{P}_j^{\text{reduced}}$ can fulfill the required load demand. There are three elimination criteria:

(i) The sum of the maximum pressure head of all pumps is smaller than required. Even a series connection of all pumps could not provide the required pressure.
(ii) The sum of the maximum volume flow of all pumps is smaller than required. Even a parallel connection of all pumps could not provide the required volume flow.
(iii) The sum of the maximum hydraulic power of all pumps is smaller than required. Even if all pumps would be operated at the point of maximum hydraulic power, it would not be sufficient.

Tuples that comply with any of these criteria are deleted immediately. This can efficiently reduce the number of tuples. Nevertheless, this excludes only a subset of all infeasible solutions.

The minimum cost are underestimated for each of the remaining tuples. Since the purchase decision for a certain pump set is fixed, the investment cost of this pump set can be calculated directly. The purchase decision for frequency converters is set to zero. We underestimate the power consumption and thus the energy cost. For each $T_j \in \mathcal{T}$ the underestimated power consumption $Po_{\mathrm{s,j}}^{\mathrm{lb,phys}}$ is calculated by the hydraulic power Po_s^{hydr} and best efficiency of any pump in the tuple $\eta_{\mathrm{best,j}}^{\mathrm{pump}}$ in every scenario $s \in \mathcal{S}$. For each tuple $j \in \mathcal{I}$ the following underestimation is valid:

$$\sum_{s\in S} W_s \sum_{i\in\mathcal{P}} po_{i,s} \geq \sum_{s\in S} W_s Po_{\mathrm{s,j}}^{\mathrm{lb,phys}} = \sum_{s\in S} W_s Po_s^{\mathrm{hydr}} / \eta_{\mathrm{best,j}}^{\mathrm{pump}}. \tag{14}$$

This corresponds to the hypothetical case that the pump with the highest efficiency provides the required hydraulic power in its best-efficiency point all alone. The resulting cost according to Obj. (5a) are underestimating the true cost and are thus a lower bound, which is based on physical principles. This consideration allows to cut off many tuples early. The power dissipated in the frequency converter is usually one order of magnitude smaller than the electrical power in the motor and is therefore neglected in this estimation.

Finally, the global primal and dual bounds are initialized in preprocessing. The global primal bound is the value of the best valid solution and is initially set to infinity. The global dual bound equals the minimum value of the lower bound of any tuple. It is initialized to the minimum of the values estimated by Eq. (14).

5.2. **Bound Improvement.** After preprocessing, the gap between the primal and dual bound is attempted to be reduced over time. On the one hand, better primal solutions are searched for. On the other hand, the minimum values of the lower bound of the tuples are improved to increase the dual bound of the overall minimization problem. If the resulting value of the lower bound of a tuple is above the global primal bound, it can be cut off.

5.2.1. *Upper Bound Search.* In order to find a new, better primal solution, the objective value of each tuple $T_j \in \mathcal{T}$ is estimated in each step. The exact MINLP is then solved for the tuple with the best estimated objective value, i.e. the most promising set of pumps.

Estimation of the Objective Value. The value of the primal solution of a tuple $T_j \in \mathcal{T}$ is estimated using a heuristic. It is assumed that the difference between the lower bound of the power consumption estimated during preprocessing $Po_{\mathrm{s,j}}^{\mathrm{lb,phys}}$, Eq. (14), and the power consumptions' exact value of the primal solution of a tuple $Po_{\mathrm{s,j}}^{\mathrm{primal}}$ is comparable for all tuples $j \in \mathcal{I}$. We calculate this difference for all tuples in $\mathcal{T}$ for which we already know the primal solution by:

$$v_{s,j} = (Po_{\mathrm{s,j}}^{\mathrm{primal}} - Po_{\mathrm{s,j}}^{\mathrm{lb,phys}})/Po_{\mathrm{s,j}}^{\mathrm{lb,phys}} \quad \forall s \in \mathcal{S}, j \in \mathcal{I}. \tag{15}$$

The expected power consumption $Po_{\mathrm{s,j}}^{\mathrm{exp}}$ of tuples for which we have not yet computed a primal solution is estimated using the mean of the deviation $v_{s,j}$ of all tuples with known primal solution:

$$\begin{aligned} \sum_{s\in S} W_s \sum_{i\in\mathcal{P}} po_{i,s} &\approx \sum_{s\in S} W_s Po_{\mathrm{s,j}}^{\mathrm{exp}} \\ &= \sum_{s\in S} W_s \left(1 + \frac{\sum_{m\in\mathcal{I}^{\mathrm{primal}}} v_{s,m}}{|\mathcal{I}^{\mathrm{primal}}|}\right) Po_{\mathrm{s,j}}^{\mathrm{lb,phys}} \quad \forall j \in \mathcal{I}\,, \end{aligned} \tag{16}$$

where $\mathcal{I}^{\mathrm{primal}} = \{j \in \mathcal{I} \,|\, \exists U_j < \infty\}$ is the indexset of tuples with finite primal solution. Based on this, the total cost is estimated according to Obj. (5a). Here, the exact known investment costs of the pumps are considered while the costs for the frequency converters are neglected.

Search for Better Primal Solution. When searching for a new primal solution, the tuple with the lowest expected cost is selected. The set of pumps is reduced to the purchased pumps $\mathcal{P}_j^{\mathrm{reduced}}$ in the selected tuple T_j. The MINLP from Sec. 4 is formulated with the reduced set of pumps and the purchase decision variables are set to $y_i = 1 \; \forall\, i \in \{1, ..., |\mathcal{P}_j^{\mathrm{reduced}}|\}$.

In general, the resulting reduced problems for the tuples in the set $\mathcal{T}$ can be solved considerably faster than the overall problem. Nevertheless, high computation times may occur for some tuples $T_j \in \mathcal{T}$. If the tuple is considered for the first time, the computation time is limited to 15 s. If a valid solution is found, the primal U_j and dual bound L_j are stored for the tuple. If the subproblem is infeasible for a tuple $T_j \in \mathcal{T}$, it is removed from the tuple list $\mathcal{T}$. If the tuple is re-selected in a later step, the computation time is increased stepwise. By this method, we try to avoid wasting computation time on sub-optimal solutions. We expect that the converged solution can already be cut off at an early stage without the need to solve the reduced problem to global optimality. In the best case, only a single reduced MINLP needs to be solved to global optimality. If a subproblem for a tuple $T_j \in \mathcal{T}$ is solved to proven global optimality, it will be deactivated for a search for further primal solutions. Unfortunately, it is not possible to continue or warm-start the computation with the selected programming framework[1] later on. Instead, the computation has to be restarted, this time with a longer maximum computation time ($\geq$ 15 s). For

[1]We implemented the algorithm in MATLAB 2019a using amongst others YALMIP [Löfberg, 2004] and OPTI Toolbox [Currie et al., 2012].

this reason, it is important to carefully select the maximum computation time for the individual steps.

If there is no promising tuple left, which we define as the lowest expected cost exceeding 120% of the global primal solution, the search for better primal solutions is no longer executed. However, the lower bound search (cf. Sec. 5.2.2) also still allows to find better primal solutions, if the reduced MINLP is solved in a later step.

5.2.2. *Lower Bound Search.* Alternating with the search for a better (i.e. lower) primal bound, the dual bound is attempted to be raised. The procedure is similar to the primal bound search: a suitable tuple is selected and a reduced optimization problem is solved. The search for a better (i.e. higher) dual bound is repeated three times before again continuing the search for a lower primal solution, as we found that it is generally more difficult than finding a better primal solution. In the dual bound search the tuple with the lowest individual dual bound $min(\mathcal{L})$ is selected (called weakest tuple). This is the weakest individual dual bound and determines the dual bound of the overall problem $L^{\text{global}} \leq min(\mathcal{L})$. To increase the overall dual bound, the dual bound of the weakest tuple has to be increased by solving the corresponding subproblem. The dual bounds for tuples that have not yet been examined are the underestimated cost of the preprocessing (cf. Eq. (14)). In turn, for tuples that have already been examined, the dual bound of the tuple from the previous step is applied.

The solved optimization problem corresponds to the one from the primal bound search with a special feature: In the first step, the piecewise linear relaxed problem (PWR MIP, cf. Sec. 4.4) of the MINLP is set up and solved instead (computation time limit of 60 s). The relaxed MIP is in general easier to solve and the so computed lower bound is often sufficient high to cut off the tuple. If the solution could not be cut off, the tuple is again selected at a subsequent loop iteration and then the reduced MINLP is solved, whereby the computation time is initially again limited to 15 s and subsequent increased in later iterations.

5.2.3. *Parallelization.* To further reduce computation times, the presented algorithm is parallelized. In each step N optimization problems are solved simultaneously on different cores: Therefore not only a single tuple with the best expected primal bound (in case of primal search) or lowest dual bound (in case of dual search) is selected, but N tuples with the best expected primal or lowest dual bounds are solved. If a tuple is solved before finishing the computation of any of the other first N tuples, the next best/weakest tuple is solved on the available core.

6. Computational Results

In this section the results of the optimization problem are discussed. First, the set of test instances, which are scenarios of high technological importance, are presented and the implementation and settings are clarified. Based on this, the performance of the different solving approaches is presented. Afterwards, a technical discussion of the results and the significance for practice is given.

6.1. Selection of Test Instances.

The previously presented different systems (Sec. 3) and the wide range of variations are analyzed carefully to choose technologically meaningful test instances. Tested instances are numerated in Tab. 4, in which the different possible physical variants are listed. For each of the buildings B1–B3 and the test rig three different topologies are considered. (i) Parallel connection of the pumps for a central booster station ($|\mathcal{F}| = 1$, Constr. (4) active), hereinafter referred to as parallel. (ii) Unrestricted topology for a central booster station ($|\mathcal{F}| = 1$, Constr. (4) not active), hereinafter referred to as central. (ii) Unrestricted topology for a decentral booster station ($|\mathcal{F}| = 5$, Constr. (4) not active), hereinafter referred to as decentral. The complexity increases significantly, respectively, due to the increasing degrees of freedom. The heuristic presented in Sec. 3.4 is used to select 15 different pump types for each of the buildings B1–B3. Each pump type can be bought up to $N^{\text{buy}} = 4$ times which leads to a total set of $|\mathcal{P}| = 15 \times 4 = 60$ pumps. For the test rig the set of pumps is limited to the $|\mathcal{P}| = 13$ available pumps (6 different types), where up to $N^{\text{buy}} = 6$ can be installed and therefore purchased. While for the buildings B1–B3 a frequency converter has to be installed additionally to allow for speed control, all considered pumps for the test rig are already equipped with frequency converters and therefore the decision to buy a frequency converter is disregarded. The characteristic curves as well as costs of the pumps and frequency converters are obtained from manufacturer data. The loss factor ζ^{inst} is determined experimentally for the test rig, whereas it is set to zero for all real buildings. The load profiles match the load profiles presented in Sec. 3.

Table 4. Instances for testing the different solution approaches.

	parallel	free topology	
		central	decentral
building 1	B1.P	B1.C	B1.D
building 2	B2.P	B2.C	B2.D
building 3	B3.P	B3.C	B3.D
test rig w/ exp. data	TRE.P	TRE.C	TRE.D

The lifetime $T = 15\,\text{a}$ for pumps is derived from the depreciation table ("AfA Table") for the sector "Energy and Water Supply" of the German Federal Ministry of Finance [AfA table]. For the interest rate $r = 2.08\,\%$ the discount rate [Bundesbank] is used with a remaining lifetime of 15 years

(7 year average, key date Aug 31st 2019). For the energy cost ($C_{\text{elect}} = 0.3, €/kWh$) the mean value of the household electricity price for the second half of 2018 in Germany is consulted [Destatis]. This results in an annuity-present value factor of $APF = \sum_{t=1a}^{T} 1/(1+r)^t = 12.77$. The pressure is calculated in bar and the volume flow in $\mathrm{m}^3\,\mathrm{h}^{-1}$. For the buildings B1–B3 the cost are calculated in k€ and the power in kW, for the test rig in € and W. Thus, the coefficients of the problem become better scaled.

The three different optimization models, namely the nonlinear (MINLP), piecewise linearized (PWL), and piecewise relaxed model (PWR), can be solved using different off-the-shelf solvers and the developed algorithm. In this work the Solvers GUROBI v8.1.1 [Gurobi Optimization, 2019], SCIP v5.0 [Gleixner et al., 2017] (using IPOPT v3.12.9 [Wächter and Biegler, 2006] and SoPlex v3.1.) and BARON v19.7.13, [Tawarmalani and Sahinidis, 2005], (using CPLEX v12.9) as well as the developed solving algorithm (AL, cf. Sec. 5.1) are trialed to compare computation time and solution quality. If nothing else is specified, default settings are used. For the PWL, 32 simplices are used for buildings B1-B3 and 50 simplices for the test rig, which are evenly distributed. We use a 1-4 orientation for each grid, as introduced in Misener and Floudas [2010]. For the PWR a discretization of $R = 6$ elements in q direction and $K = 3$ elements in n direction for the pressure and $R = 5$, $K = 5$ for the power is used for real buildings. For the test rig a discretization of $R = 6$, $K = 2$ for the pressure and $R = 4$, $K = 4$ for the power is used.

The optimization model was implemented in Matlab 2019a using YALMIP [Löfberg, 2004]. The solver SCIP is interfaced via the OPTI toolbox [Currie et al., 2012]. For all other solvers, manufacturer interfaces are used. The algorithm presented in Sec. 5.1 has also been developed and executed in Matlab 2019a. All computations were performed on a Windows 10 machine with an Intel i7-8700 CPU (6 cores @3.20GHz) and 16GB RAM. ε-optimality (with $\varepsilon = 0.1$) is tried to be achieved within an time limit of 3 hours.

6.2. **Performance of Different Solution Approaches.** To compare the different solution approaches and solvers, for each variant the instances given in Tab. 4 are computed. A large part of the instances have a gap $> \varepsilon$, which is why a comparison of the gap at the end of the computation time is used. As in Pecci et al. [2019], the share of solved instances with a gap smaller δ, $\rho(\delta) = 100\,(\#\,\text{instances with gap} \leq \delta)/(\#\,\text{test instances})$, is plotted for the remaining gap δ, cf. Fig. 8.

Comparison of MINLP and MIP. The comparison of the directly solved MINLP with the directly solved PWL-MIP and the PWR-MIP (cf. Fig. 8a) shows that more instances can be solved with a satisfactory gap by using the MIP.

The difference between SCIP and BARON to directly solve the MINLP is not significant. Both solvers can only solve 1/12 of the instances with a gap $\leq \varepsilon$. In addition, we encountered occasionally errors with both solvers during the solution process. For SCIP this can be reduced by a less aggressive presolving. A more detailed discussion can be found in Appendix A. A direct solution of the MINLP with off-the-shelf solvers is due to the large

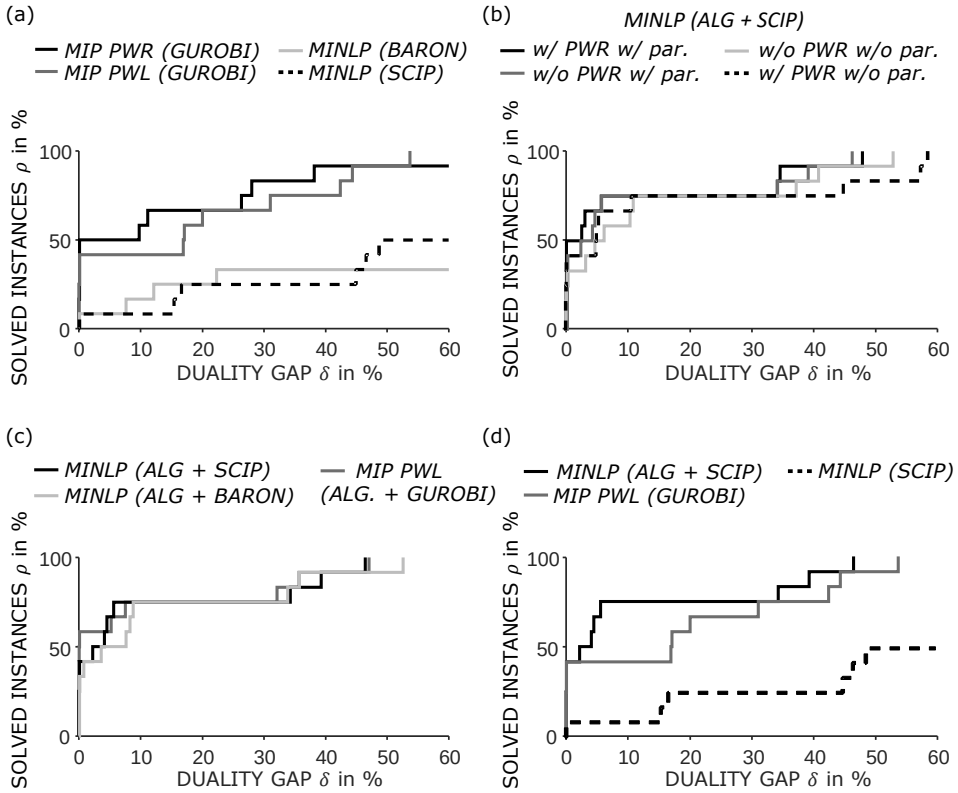

FIGURE 8. Solved instances $\rho(\delta)$ with a gap smaller δ for different solution approaches. Comparison of (a) directly solved MINLP, PWL and PWR, (b) different options of developed algorithm, (c) different solvers for the developed algorithm (settings: w/ PWR, w/par.), and (d) directly solved MINLP, directly solved PWL and MINLP solved using the developed algorithm (settings: w/ PWR, w/par.).

duality gap and potential wrong results not a suitable approach. In the developed algorithm the individual problems are smaller and errors by SCIP or BARON were rare. However, for SCIP the presolving-emphasis settings for the calculation with the developed algorithm were set to "fast" to avoid any problems.

The PWL-MIP is an approximation of the MINLP. The relative deviation between the primal solution of the PWL-MIP and the best known primal MINLP solution (calculated for the MINLP with the developed algorithm) is on average 3.6 % for all 12 instances. For solutions with a gap of $\leq \varepsilon$ (4/12 instances) the deviation is 1.65 %. For 2/12 instances, the same pumps and FCs are purchased as for the best known MINLP solution. If the PWL-MIP is solved using the developed algorithm, lower gaps can be achieved (see Fig 8c). In this case the mean deviation is 1.61 % (all instances) or 1.75 % (instances with gap $\leq \varepsilon$) and the investment decisions are the same for 5/12 instances. In comparison to the direct solution of the MINLP, more useful

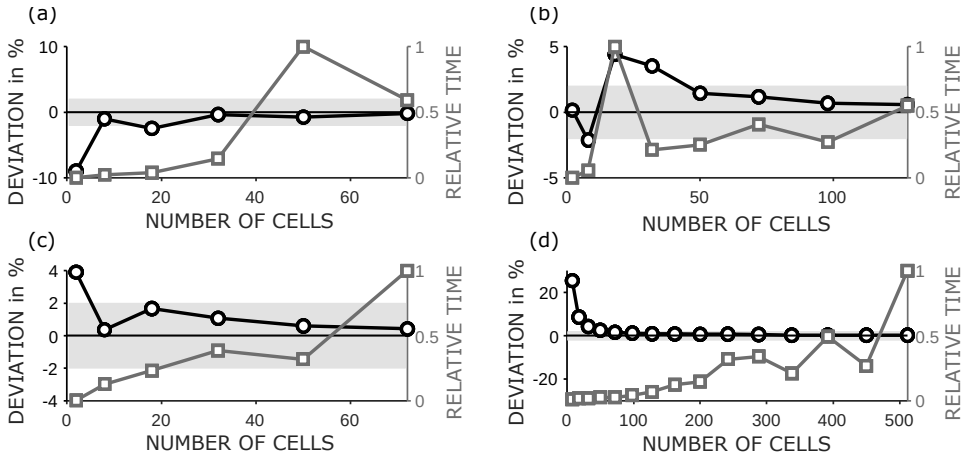

FIGURE 9. Influence of grid size on deviation to MINLP solution and computation time. The 2 % limit is highlighted in gray.

solutions can be achieved and the approximation quality is acceptable with around 2 % for the given discretization. However, high computation times and large duality gaps still result, especially when using an off-the-shelf solver.

The influence of the discretization is investigated using the comparatively simple instances with only parallel pump configurations (B1.P, B2.P, B3.P, TRE.P). Fig. 9 shows the deviation from the best known MINLP solution and the normalized computation time over the number of cells. The deviation converges towards 0, whereby the computation time increases as a trend. Partly an overestimation, partly an underestimation of the objective value of the MINLP occurs. On the basis of the investigation, 32 elements for real buildings and 50 for the test rig are selected. With an average deviation of less than 2 % (corresponding with the order of magnitude of the measurement errors on the test rig), the level of detail is sufficient.

The dual solution of the PWR-MIP is compared with the best found primal MINLP solution: For solutions with a gap $\leq \varepsilon$ (6/12 instances) the deviation is 7.0 % or 19.91 % (all instances) and investment decisions are the same for 5/12 of the instances. The high deviation is due to non-converged solutions for difficult instances. In this case, the dual bound of the PWR-MIP cannot be raised sufficiently, which is why it serves only as a weak lower bound.

Performance of Developed Algorithm. Fig. 8 (b) shows the performance of the developed algorithm with and without the use of PWR (w/ PWR and w/o PWR) and parallelization (w/ par. and w/o par.). Without the use of PWR, the reduced MINLP is already solved within the first selection of a tuple, thus the PWR-MIP is not solved before. Without parallelization, only one tuple is solved instead of N tuples at the same time. SCIP is used as MINLP solver and GUROBI as PWR-MIP solver. All in all, the deviations of the different settings are rather small. The results show:

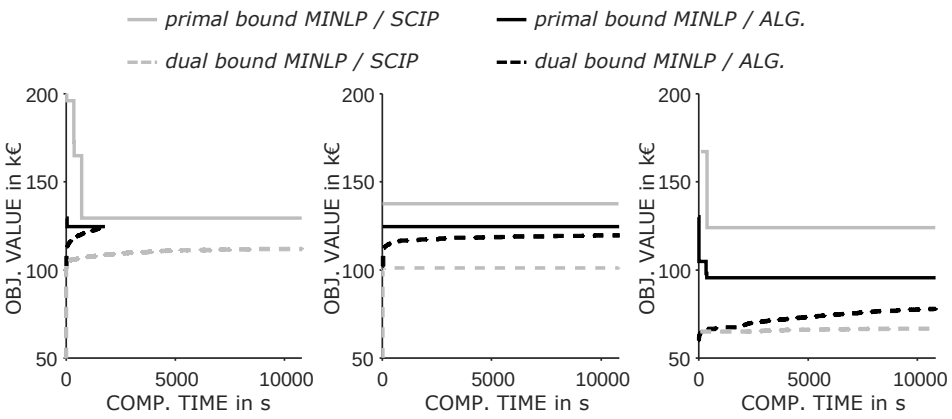

FIGURE 10. Comparison of the progression of the primal and dual bound for the developed algorithm (SCIP, w/ PWR, w/ par.) and the directly solved MINLP (SCIP, presolving "fast") for the instances (a) B2.P, (b) B2.C and (c) B2.D.

- The use of PWR shows only minor improvements. This could be caused by a too fine discretization, resulting in a dual bound of the PWR that can only be computed with high effort.
- The parallelization offers a slight performance increase. The reason it only yields small improvements could be that when solving N tuple at the same time, the computation of one tuple takes much longer than for the others. As long as the first N tuples are not finished, the primal and dual bounds are not updated. This holds the risk of wasting time on the computation of tuples which are cut off later. In addition, parallelization causes computational overhead.

In Fig. 8 (c), BARON and SCIP are compared as underlying MINLP solvers for the developed algorithm (w/ PWR, w/ par.). The performance of SCIP is slightly better. In addition, the PWL-MIP is solved with the developed algorithm (GUROBI as PWL-MIP solver, w/o PWR, w/ par.). The performance is slightly below that of the MINLP. A possible cause is the computational overhead of the algorithm: The optimization model has to be set up for each tuple. This is more complex for the PWL model due to the increased number of equations, which can lead to a loss of performance. Compared to directly solving the PWL-MIP, considerably more instances can be solved (cf. Fig. 8 (a)).

Concluding the results for the developed algorithm (SCIP, w/ PWR, w/ par.) are compared with directly solved MINLP and PWL-MIP in Fig. 8 (d): the developed algorithm allows to solve 50% of the instances with a gap $\leq \varepsilon$ and all instances with a gap $\leq 48\%$. This is substantially more than directly solving the MINLP and also than directly solving the approximated PWR-MIP.

The progression of the dual and primal bound for the developed algorithm (SCIP, w/ PWR, w/ par.) and the directly solved MINLP (SCIP, presolving "fast") is shown in Fig. 10. The complexity of the problem increases from

(a) (B2.P) to (b) (B2.C) to (c) (B2.D). The developed algorithm finds the optimal primal solution very fast and at all time steps the primal bound as well as the dual bound of the developed algorithm is better than for the directly solved MINLP.

6.3. **Technical Discussion of the Optimized Booster Station Designs.** In the following, the technical aspects of the solutions are discussed. In this section, we always refer to the best found primal solution of any solver.

Tab. 5 summarizes the relevant aspects of the optimization results for all instances. The following conclusions can be drawn:

- For central booster stations the restriction of the topology to solely parallel connections has no disadvantage for the tested real buildings. This may be due to the selected pump kit, since the existing pumps are designed for parallel connections. For the test rig, the central solution (unrestricted topology) is slightly superior.
- 20–25% of the total cost can be saved with decentralized systems. The system performance increases by 50% up to 100%. The latter corresponds to halving the required power. This requires higher investment costs and more pumps, which is far outweighed by the energy savings.
- Although the load cases could already be covered by a single pump, always 2–4 pumps are bought due to the achieved energy savings. In some cases different pump types are used, in others (B3.P, B3.C) solely one pump type is used. Only about half of the pumps are equipped with FCs.

For building B3, the actual installed pumps are known. In the installed system four parallel connected pumps of the same type (all with FC) are used. This investment decision is fixed and the speed optimized (see column "inst." in Tab. 5). In comparison, approx. 50% of the total cost can be saved by optimizing the investment costs and speed at the same time. Even if costs for an additional redundant spare pump are taken into account (2053 €, without FC), 32 % of the total cost can still be saved.

All selected pumps are highlighted in Fig. 11. We use dashed black lines for all pumps in all three considered buildings, which are used in the decentralized layout, while we use solid black lines for all pumps, that are used in the centralized and/or parallel setting. All pump labels in Fig. 11 (a) and (d) are based on the hydraulic power. The same pumps where selected for all buildings in the central and parallel case, as shown by the solid black lines, while at the test rig different combinations of pumps are used in the central, parallel and decentral layout. More details about the derived topologies for the test rig are shown in Sec. 7 and Fig. 14. Detailed results for the first building (B1) are given as well in Fig. 12.

For building B1, the optimal topologies are shown in Fig. 12. The central topology (a) shows that only the largest pump is equipped with a frequency converter and operates for every load scenarios. For the load cases with higher power demand, further pumps are switched on additionally. Since they only run for a small part of the time and thus their energy consumption

TABLE 5. Results of the best found primal solution for each instance.

	building B1			building B2		
	parallel	central	decen.	parallel	central	decen.
total cost in k€	141.7	141.7	107.4	124.4	124.4	93.9
rel. total cost in %	100	100	75.8	100	100	75.5
invest. cost in k€	32.4	32.4	34.7	30.3	30.3	32.4
# pumps	3	3	4	2	2	4
# diff. types	2	2	4	2	2	4
# FC	1	1	3	1	1	2
mean power in kW	10.9	10.9	7.2	9.3	9.3	6.1
η_{sys}[2] in %	37.8	37.8	56.9	36.6	36.7	56.1

	building B3				test rig TE		
	parallel	central	decen.	inst.	parallel	central	decen.
total cost in €	16 377	16 377	12 715	24 391	957	933	780
rel. total cost in %	100	100	77.6	148.9	100	97.5	81.5
invest. cost in €	6 321	6 321	7 762	14 868	276	244	226
# pumps	2	2	4	4	2	2	2
# diff. types	1	1	2	1	2	2	2
# FC	1	1	2	4	–	–	–
mean power in W	998	998	491	947	67.6	68.4	55
η_{sys}[1] in %	22.4	22.4	45.5	23.64	25.7	25.4	31.5

is less important, they are not equipped with a frequency converter. A complex topology results for the decentralized solution (b). In scenarios with low hydraulic power demand, one pump solely supplies the pressure zones 1 and 2. Two pumps connected in series supply the upper pressure zones. After the first pump a partial volume flow is branched off to supply pressure zone 3. Only for load cases 4 and 5 a further pump is switched on, which has no frequency converter.

The trade-off between investment costs and energy costs for building B1 is shown by the Pareto front in Fig. 13. The computation was done using the ϵ-constraint method [Ehrgott, 2005, pp. 98-101], in which the maximum power consumption was added as a constraint. The investment costs were weighted very high by setting the lifetime to 1 month. The optimization was performed with different upper limits on the power consumption. The Pareto front of the parallel and central topologies coincide exactly. The decentralized solution completely dominates either central solution. The minimum necessary power, calculated by hydraulic power and component efficiency, can almost be reached. This indicates a good choice of the pump kit and thus confirms the heuristics in Alg. 1. The optimal solution discussed before (lifetime of 15 years), is in the range of high energy weighting. It should be noted that the computation time for high weights for the energy increases significantly, since fewer solutions can be cut off.

7. VALIDATION

In order to validate the methodology, assumptions and models, the results obtained for the test rig (Sec. 3.2) are experimentally examined. The boundary conditions applied for the optimization are obtained in two different ways. In case (i), the loss factor ζ_{loss} and the required pressure increase in

[2]The system efficiency is defined as: $\eta_{\text{sys}} := \frac{Po^{\text{mean}}_{\text{hydr,dec.}}}{Po_{\text{mean}}} = \frac{\sum_{s\in\mathcal{S}} W_s Po_{s,\text{hydr,dec.}}}{\sum_{s\in\mathcal{S}} W_s \sum_{i\in\mathcal{P}} po_{i,s}}$

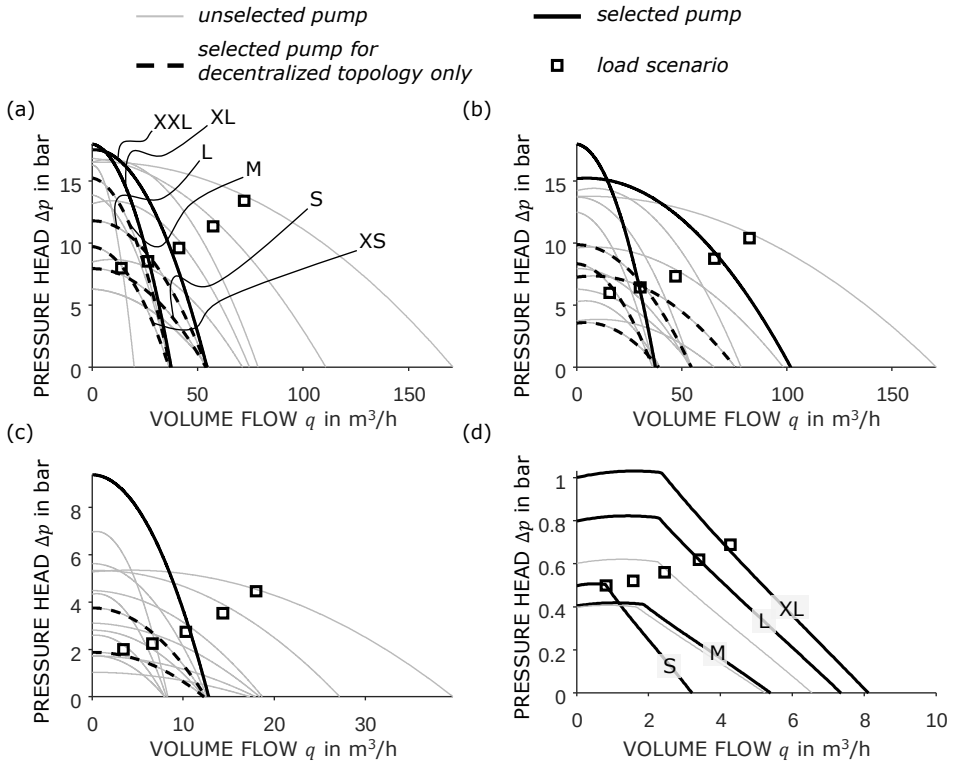

FIGURE 11. Selected pumps after optimization for each building and the test rig. The shown pump size is based on the maximum power. (a) building B1 (b) building B2 (c) building B3 (d) test rig. The size indication (XS - XXL) refers to the maximum hydraulic power of the pumps.

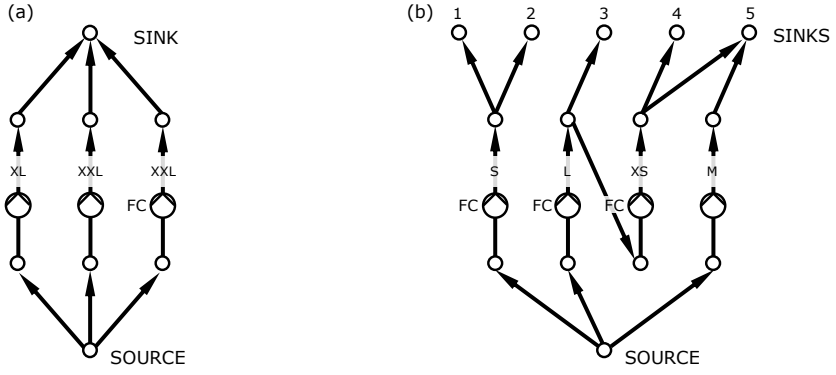

FIGURE 12. Optimal topology for the instances (a) B1.P/C and (b) B1.D.

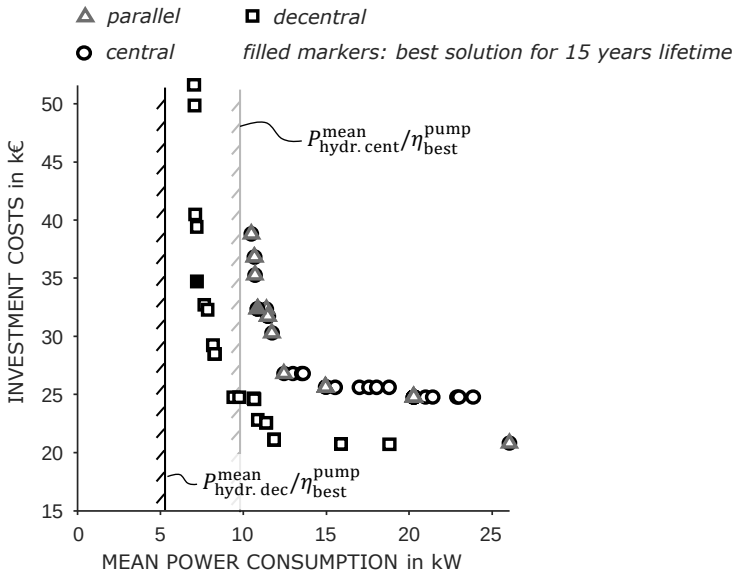

FIGURE 13. Pareto Front of the objective's investment cost and power consumption for the instances B1.P, B1.C and B1.D. The filled markers represent the best solution for a lifetime of 15 years (corresponds to Tab. 5).

the load scenarios are determined experimentally. For case (ii), a hydraulic model is developed, for which the friction coefficients of the components are estimated on the basis of data given in literature [GF Piping System, 2019, Idelchik, 2007]. The latter case is the more practical case, since experimental surveys cannot always be carried out in the field. In both cases, manufacturer specifications are used for the characteristic curves of the pumps and a strictly quadratic relationship between pressure losses and the volume flow is assumed. It should be noted that not all friction influences can be taken into account in the model. Depending on the topology, elbow and tee fittings are necessary to achieve the desired configuration, which are not taken into account in the optimization model. For a more detailed investigation of the friction influence, we refer to Müller et al. [2019a].

The optimal topologies are shown in Fig. 14. Only for the central booster station (b)/(c) there are deviations in the optimal topology between experimental and literature data. Without the use of experimental data, the pressure losses are assumed to be lower, which is why slower rotational speeds are applied.

The shown topologies are set up on the test rig, trying to keep the pressure losses due to the layout of the connection as low as possible. For every scenario the rotational speeds are applied and the valves are set so that the same volume flow is achieved on each floor. The pumps run at a constant speed, i.e. without control-loop.

In Fig. 15, the power consumption (measure for the achievement of the objective) is plotted against the volume flow (measure for the satisfaction of the load demand) for all topologies and scenarios.

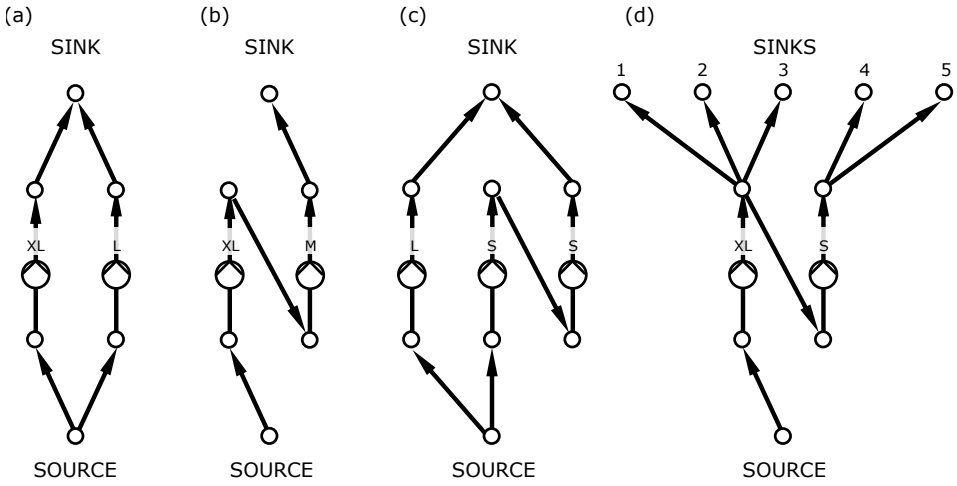

FIGURE 14. Optimal topology for the test rig: (a) parallel (experimental data as well as solely literature data), (b) central (experimental data), (c) central (solely literature data) and (d) decentral (experimental data as well as solely literature data). For topology (c) the setup on the test rig is shown in Fig. 3.

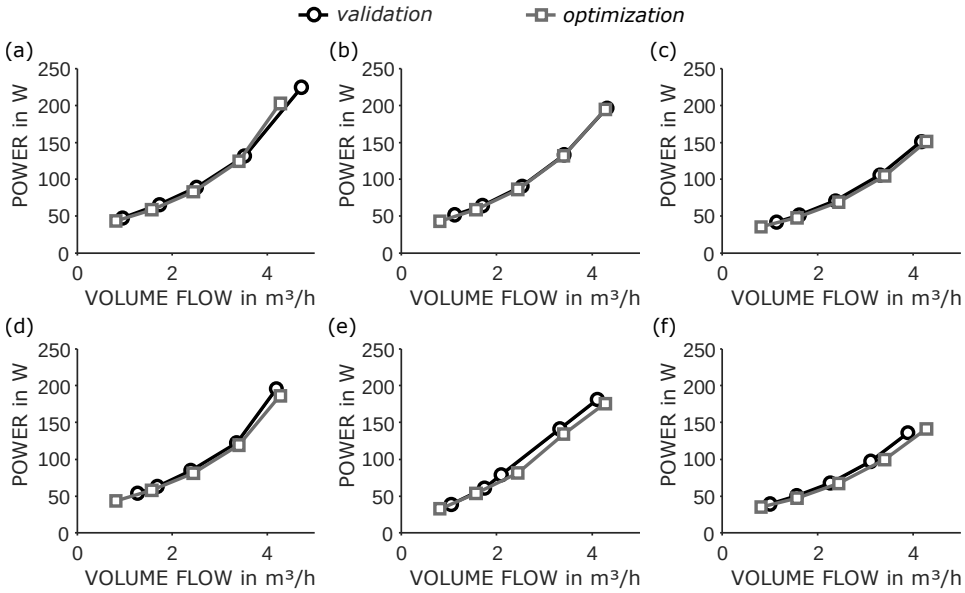

FIGURE 15. Power consumption over volume flow for optimization and validation results for all five load scenarios. Results based on experimental data for (a) parallel (b) central and (c) decentral topologies, and based on literature data for (d) parallel (e) central and (f) decentral topologies are shown. The error bars are covered by the markers.

The correlation between power and volume flow is well matched in experiment and validation even though there is a deviation between the required and the measured volume flows. As expected, the correlation is higher when using the experimental data.

Furthermore, the mean volume flow,

$$Q_{\text{mean}} := \sum_{s\in\mathcal{S}} W_s \sum_{f\in\mathcal{F}} q_{f,s}, \tag{17}$$

the mean power consumption,

$$Po_{\text{mean}} := \sum_{s\in\mathcal{S}} W_s \sum_{i\in\mathcal{P}} po_{i,s}, \tag{18}$$

and the geodetic system efficiency are investigated cf. Tab. 6,

$$\eta_{\text{geo}} := \frac{\sum_{s\in\mathcal{S}} W_s \varrho g \sum_{fin\mathcal{F}} \Delta h_f q_{f,s}}{Po_{\text{mean}}}. \tag{19}$$

The values are calculated using the density $\varrho = 998\,\mathrm{kg\,m^{-3}}$, the gravitational acceleration $g = 9.81\,\mathrm{m\,s^{-2}}$, and the geodetic height difference $\Delta h_f = \{1\,\mathrm{m}, \ldots, 5\,\mathrm{m}\}$ for the different pressure zones. The geodetic system efficiency η_{geo} is a measure for the deviation of the energy cost and is used to determine the expected total cost:

$$C^{\text{exp}}_{\text{total}} := C^{\text{opt}}_{\text{invest}} + C^{\text{opt}}_{\text{energy}} \left(1 + \frac{\eta^{\text{opt}}_{\text{geo}} - \eta^{\text{exp}}_{\text{geo}}}{\eta^{\text{opt}}_{\text{geo}}}\right). \tag{20}$$

The results show that the mean volume flow is higher than demanded, i.e. the pressure losses have been overestimated. As a result, the power consumption is also higher than predicted. In practice, the deviations would be compensated by a closed loop control of the pumps' rotational speed. The systems are nevertheless comparable on the basis of the geodetic efficiency, which is slightly lower than assumed in the optimization. The deviation is smaller for the pump model based on the experimental data. For the instances where the pump S was installed (cf. Fig. 14 (b) and (c)), the deviation is higher, which indicates inaccuracies in the used characteristics of pump S (given by the manufacturers data sheet). In spite of these uncertainties, the total costs are lower for decentralized systems. The deviations in efficiency (5-10%) are significantly smaller than the saving potential compared to conventional parallel design ($\approx 50\%$, cf. Tab. 5). In addition, deviations are also to be expected for the conventional design. This shows that mathematical optimization is suitable for the planning of pumping system design and operation and that the level of detail realized in the models is sufficient.

TABLE 6. Comparison of optimization an validation results.

		parallel	central	decentral
experimental data	$Q^{\text{opt}}_{\text{mean}}$ in $\text{m}^3\,\text{h}^{-1}$	1.732	1.732	1.732
	$Q^{\text{exp}}_{\text{mean}}$ in $\text{m}^3\,\text{h}^{-1}$	1.877 ± 0.027	1.895± 0.027	1.817± 0.026
	deviation in %	8.34	9.39	4.88
	$Po^{\text{opt}}_{\text{mean}}$ in W	67.578	68.448	55.043
	$Po^{\text{exp}}_{\text{mean}}$ in W	74 ±2.36	74.16±1.78	58.86 ±1.77
	deviation in %	9.51	8.35	6.94
	$\eta^{\text{opt}}_{\text{geo}}$ in %	18.292	18.06	22.458
	$\eta^{\text{exp}}_{\text{geo}}$ in %	17.88	17.632	21.218
	deviation in %	-2.26	-2.37	-5.52
	$C^{\text{opt}}_{\text{total}}$ in €	957.3	933.7	780.6
	$C^{\text{exp}}_{\text{total}}$ in €	972.6	950	811.3
literature data	$Q^{\text{opt}}_{\text{mean}}$ in $\text{m}^3\,\text{h}^{-1}$	1.732	1.732	1.732
	$Q^{\text{exp}}_{\text{mean}}$ in $\text{m}^3\,\text{h}^{-1}$	1.893± 0.027	1.802± 0.026	1.715 ± 0.026
	deviation in %	9.32	4.05	-0.98
	$Po^{\text{opt}}_{\text{mean}}$ in W	66.298	62.148	53.953
	$Po^{\text{exp}}_{\text{mean}}$ in W	72.574±2.36	67.202 ±2.36	56.318 ±1.77
	deviation in %	9.47	8.13	4.38
	$\eta^{\text{opt}}_{\text{geo}}$ in %	18.646	19.891	22.912
	$\eta^{\text{exp}}_{\text{geo}}$ in %	17.696	18.343	21.02
	deviation in %	-5.1	-7.78	-8.26
	$C^{\text{opt}}_{\text{total}}$ in €	944.4	919.4	769.7
	$C^{\text{exp}}_{\text{total}}$ in €	978.4	968.1	814.5

8. Conclusion and Outlook

We presented three different modeling approaches for the optimization of booster stations in high-rise buildings. The underlying optimization model is mostly linear in its decision variables, but the consideration of the pump characteristics for the booster station design leads to a nonconvex Mixed-Integer Nonlinear Program, which is hard to solve for real-world instances in its original form. To overcome this drawback, we derived two additional model variants, allowing for MIP formulations. These are a piecewise linear approximation and a piecewise linear relaxation of the nonlinear pump characteristics. Furthermore, we implemented a problem-specific algorithm which is based on these different methods and additional domain-specific engineering knowledge to derive global-optimal optimization results for real-world instances efficiently. The algorithm reduces the original MINLP by fixing specific pump purchase decisions and uses a selection heuristic to find feasible primal solutions in a very short time. This primal solution search is undertaken alternating with the dual solution search, which is based either on the reduced MINLP directly or on the implemented piecewise linear relaxation. The shown algorithm improves the solution times considerably in

comparison to the original MINLP formulation. We presented the computation benefits of the developed algorithm for three different high-rise buildings as well as for a test rig. The test rig, constructed for validation purposes, represents the scaled water supply in a high-rise building. Therefore, we were able to conduct experiments for the different optimization results for the optimization models of different degree of detail. The comparison of optimization and experimental results on the test rig shows that the degree of detail is adequate and that the introduced method is transferable to real-world infrastructure. Allowing for different degrees of freedom for the alignment of pumps in the water supply system shows that the decentralized topology of booster stations can yield approx. 25% of cost savings when compared to an optimized parallel pump alignment. The latter design is the current common practice. Additionally, frequency converters were installed for only approx. half of the pumps in booster stations, which is due to the trade-off of energy costs in operation and investment costs making up total cost. Compared to a conventionally designed booster station, the mathematical optimization could achieve a total cost reduction of up to approx. 50%. These results show that we were able to derive significantly improved system designs by combining domain-specific engineering knowledge and discrete optimization methods. The developed approach assists engineers as early as in the design stage to improve the system design. This is possible, since this approach allows to consider the real load profile in the implemented two-stage stochastic optimization problem. For the future, we want to address further open research questions in this area, both in the algorithmic and engineering domain. For instance, to obtain reasonable problem sizes, we had to reduce the number of different pump types in the preprocessing with the help of an engineering knowledge applying heuristic. Therefore, improving the performance of the algorithm to consider more pumps could achieve even better system designs. This objective could be approached by an improved deployment of the underlying piecewise relaxation. From an engineering perspective, we want to examine more complex, branched systems and want to look into the transfer of the methods proven promising to different fluid systems.

Acknowledgments. The presented results were partly obtained within the research project "Exact Global Topology-Optimization for Pumping Systems", project No. 19725 N/1, funded by the program for promoting the Industrial Collective Research (IGF) of the German Ministry of Economic Affairs and Energy (BMWi), approved by the Arbeitsgemeinschaft industrieller Forschungsvereinigungen Otto von Guericke e.V. (AiF). We want to thank all the participants of the working group for the constructive and close collaboration. Moreover, we thank the German Research Foundation, DFG, for partial funding within the Collaborative Research Center CRC 805 "Control of Uncertainties in Load-Carrying Structures in Mechanical Engineering", project No. 57157498. In addition to that, we appreciate the partial funding by the KSB Stiftung Stuttgart, Germany.

Appendix A. Appendix

Within the computational evaluations we encountered problems with the two MINLP solvers SCIP (v5.0) and BARON (v.19.7.13), which we present in more detail in the following. Within modeling, we put a lot of effort in the conditioning of the underlying optimization problem to reduce errors based on an ill-conditioned optimization problem. A summary can be found in Tab. 7. While BARON occasionally generated no output for specific instances, SCIP either indicated larger dual bounds than the value of the true primal solutions or declared instances as infeasible, while we were able to derive feasible solutions either with BARON or manually by engineering knowledge. BARON terminated without solution output for 4/12 instances for the original MINLP given by (5) and (6). SCIP output an incorrect solution for 5/12 instances in the original MINLP with default presolving settings. We were able to reduce the number of false results for SCIP by adjusting the presolving emphasis settings to "fast" or "off", as indicated in Tab. 7. A newer version of SCIP can potentially solve the encountered issues.

Table 7. Specification of the instances for which an error occurred in the direct solution of the MINLPs.

	BARON	SCIP		
presolving emphasis settings	default	default	fast	off
no output	B1.P, B1.D, B2.C, B2.D	–	–	B1.P
wrongly detected infeasibility	–	B1.P, B1.D, B3.P	–	TE.D
indicated to large dual bound	–	B3.C, B3.D	B2.P	–
# instances with error	4/12	5/12	1/12	2/12

References

AfA table. Afa table for the branch energy and water supply. (tax depreciation for wear and tear), 1995. File number IV A 8-S 1551-9/95, 45-S 1551-20.

Lena C Altherr, Philipp Leise, Marc E Pfetsch, and Andreas Schmitt. Resilient layout, design and operation of energy-efficient water distribution networks for high-rise buildings using MINLP. *Optimization and Engineering*, 20(2):605–645, 2019.

Christopher E Brennen. *Hydrodynamics of pumps*. Cambridge University Press, 2011.

Bundesbank. Discount rates in accordance with section 253 (2) HGB, 7-year average, remaining time 15 years, 2019. Time series BBK01.WX0037.

Claus C Carøe and Jørgen Tind. L-shaped decomposition of two-stage stochastic programs with integer recourse. *Mathematical Programming*, 83 (1-3):451–464, 1998.

B Coelho and A Andrade-Campos. Efficiency achievement in water supply systems – A review. *Renewable and Sustainable Energy Reviews*, 30:59–84, 2014.

CTBUH. 2018 tall building year in review. Technical report, Council on Tall Buildings and Urban Habitat, 2018.

Jonathan Currie, David I Wilson, Nick Sahinidis, and Jose Pinto. OPTI: Lowering the barrier between open source optimizers and the industrial MATLAB user, 2012. URL https://www.inverseproblem.co.nz/OPTI/. Accessed Oct 29th 2019.

Destatis. Daten zur Energiepreisentwicklung. Lange Reihen von Januar 2005 bis August 2019, 2019.

DIN 1988-300. Codes of practice for drinking water installations – Part 300: Pipe sizing; DVGW code of practice, 2012.

DIN 1988-500. Codes of practice for drinking water installations – Part 500: Pressure boosting stations with RPM-regulated pumps; DVGW code of practice, 2011.

Matthias Ehrgott. *Multicriteria optimization*, volume 2. Springer Berlin Heidelberg, 2005.

EN 16480:2016. Pumps - minimum required efficiency of rotodynamic water pumps., 2016.

Fernando JTE Ferreira, João AC Fong, and Anibal T de Almeida. Eco-analysis of variable-speed drives for flow regulation in pumping systems. *IEEE Transactions on Industrial Electronics*, 58(6):2117–2125, 2010.

D Scott Fisher. The impact of safety factors on pump performance and selection: Case study, a methodology for correcting pump oversizing/discussion. *ASHRAE Transactions*, 107:584, 2001.

Vijay K Garg. *Applied computational fluid dynamics*. CRC Press, 1998.

Björn Geißler, Alexander Martin, Antonio Morsi, and Lars Schewe. Using piecewise linear functions for solving MINLPs. In Jon Lee and Sven Leyffer, editors, *Mixed Integer Nonlinear Programming*, pages 287–314, New York, 2012. Springer. ISBN 978-1-4614-1927-3.

GF Piping System. JRG Sanipex MT - Technical documentation, 2019. URL https://www.gfps.com/appgate/ecat/common_flow/10006Q/CH/en/231565/download/document.html. Accessed Oct 30th 2019.

Ambros Gleixner, Leon Eifler, Tristan Gally, Gerald Gamrath, Patrick Gemander, Robert Lion Gottwald, Gregor Hendel, Christopher Hojny, Thorsten Koch, Matthias Miltenberger, Benjamin Müller, Marc E. Pfetsch, Christian Puchert, Daniel Rehfeldt, Franziska Schlösser, Felipe Serrano, Yuji Shinano, Jan Merlin Viernickel, Stefan Vigerske, Dieter Weninger, Jonas T. Witt, and Jakob Witzig. The SCIP Optimization Suite 5.0. Technical report, Optimization Online, December 2017. URL http://www.optimization-online.org/DB_HTML/2017/12/6385.html. Accessed Oct 29th 2019.

Stefan Gössling, Paul Peeters, C Michael Hall, Jean-Paul Ceron, Ghislain Dubois, Daniel Scott, et al. Tourism and water use: Supply, demand, and security. an international review. *Tourism management*, 33(1):1–15, 2012.

TF Groß, PF Pöttgen, and Peter F Pelz. Analytical approach for the optimal operation of pumps in booster systems. *Journal of Water Resources*

Planning and Management, 143(8):04017029, 2017.

Johann Friedrich Gülich. *Kreiselpumpen: ein Handbuch für Entwicklung, Anlagenplanung und Betrieb*. Springer-Verlag, 2013.

LLC Gurobi Optimization. Gurobi optimizer reference manual, v8.1.1, 2019. URL http://www.gurobi.com. Accessed Oct 29th 2019.

Michael Hartisch, Alexander Herbst, Ulf Lorenz, and Jonas Benjamin Weber. Towards resilient process networks-designing booster stations via quantified programming. In *Applied Mechanics and Materials*, volume 885, pages 199–210. Trans Tech Publ, 2018.

Manuel Herrera, Edo Abraham, and Ivan Stoianov. A graph-theoretic framework for assessing the resilience of sectorised water distribution networks. *Water Resources Management*, 30(5):1685–1699, 2016.

Rainer Hirschberg. Lastprofil und Regelkurve zur energetischen Bewertung von Druckerhöhungsanlagen (DEA). *HLH Lüftung/Klima, Heizung/Sanitär, Gebäudetechnik*, pages 1436–5103, 2014.

Jesco Humpola and Armin Fügenschuh. Convex reformulations for solving a nonlinear network design problem. *Computational Optimization and Applications*, 62(3):717–759, 2015.

I. E. Idelchik. *Handbook of hydraulic resistance*. Begell House, New York, 4th ed. edition, 2007. ISBN 9781567002515.

ISO/ASME 14414. Pump system energy assessment, 2019.

David Japikse, William D Marscher, and Raymond B Furst. Centrifugal pump design and performance. *Wilder, VT: Concepts ETI, Inc, 1997.*, 1997.

Sebastian Lang, Gerhard Ludwig, Peter F Pelz, and Bernd Stoffel. General methodologies of determining the energy-efficiency-index of pump units in the frame of the extended product approach. In *Proceedings of the 8th International Conference on Energy Efficiency in Motor Driven Systems (EEMODS)*, 2013.

Eduardo Larralde and Rafael Ocampo. Centrifugal pump selection process. *World Pumps*, 2010(2):24–28, 2010a.

Eduardo Larralde and Rafael Ocampo. Pump selection: a real example. *World Pumps*, 2010(3):28–33, 2010b.

Philipp Leise and Lena C Altherr. Optimizing the design and control of decentralized water supply systems – A case-study of a hotel building. In *International Conference on Engineering Optimization*, pages 1241–1252. Springer, 2018.

Johan Löfberg. YALMIP: A toolbox for modeling and optimization in MATLAB. In *Proceedings of the CACSD Conference*, 2004.

Marvin Meck, Tim M Müller, Lena C Altherr, and Peter F Pelz. Designing an Efficient and Cost-Optimal Industrial Cooling System Using Mixed-Integer Nonlinear Programming. In *Operations Research Proceedings 2019*. Springer, 2019. To appear.

Markéta Mikolajková, Henrik Saxén, and Frank Pettersson. Linearization of an MINLP model and its application to gas distribution optimization. *Energy*, 146:156–168, 2018.

R. Misener and C. A. Floudas. Piecewise-linear approximations of multidimensional functions. *Journal of Optimization Theory and Applications*,

145(1):120–147, 2010. ISSN 1573-2878. doi: 10.1007/s10957-009-9626-0.

Ruth Misener and Christodoulos A Floudas. Global optimization of mixed-integer quadratically-constrained quadratic programs (MIQCQP) through piecewise-linear and edge-concave relaxations. *Mathematical Programming*, 136(1):155–182, 2012.

Ruth Misener and Christodoulos A Floudas. GloMIQO: Global mixed-integer quadratic optimizer. *Journal of Global Optimization*, 57(1):3–50, 2013.

Ruth Misener and Christodoulos A Floudas. ANTIGONE: algorithms for continuous/integer global optimization of nonlinear equations. *Journal of Global Optimization*, 59(2-3):503–526, 2014.

Ruth Misener, Chrysanthos E Gounaris, and Christodoulos A Floudas. Global optimization of gas lifting operations: A comparative study of piecewise linear formulations. *Industrial & Engineering Chemistry Research*, 48(13):6098–6104, 2009.

Antonio Morsi, Björn Geißler, and Alexander Martin. Mixed integer optimization of water supply networks. In *Mathematical optimization of water networks*, pages 35–54. Springer, 2012.

Tim M Müller, Lena C Altherr, Philipp Leise, and Peter F Pelz. Optimization of pumping systems for buildings: Experimental validation of different degrees of model detail on a modular test rig. In *Operations Research Proceedings 2019*, Dresden, Germany, 2019a. Springer. To appear.

Tim M Müller, Philipp Leise, Tobias Meck, Lena C Altherr, and Peter F Pelz. Systemic Optimization of Booster Stations - From Data Collection to Validation. In *International Rotating Equipment Conference (IREC) 2019*, Wiesbaden, Germany, 2019b.

Jens Norgaard and Anders Nielsen. Water supply in tall buildings: Roof tanks vs. pressurised systems. *Grundfos Water Boosting, Denmark*, 2010.

Dimitri Nowak, Helene Krieg, Michael Bortz, Christian Geil, Axel Knapp, Harald Roclawski, and Martin Böhle. Decision support for the design and operation of variable speed pumps in water supply systems. *Water*, 10 (6), 2018. ISSN 2073-4441. doi: 10.3390/w10060734.

Filippo Pecci, Edo Abraham, and Ivan Stoianov. Global optimality bounds for the placement of control valves in water supply networks. *Optimization and Engineering*, 20(2):457–495, 2019.

Gerulf KM Pedersen and Zhenyu Yang. Efficiency optimization of a multi-pump booster system. In *Proceedings of the 10th annual conference on Genetic and evolutionary computation*, pages 1611–1618. ACM, 2008.

Pavel Popela. Stochastic programming models for engineering design problems. *Eng. Mech.*, 17(5-6):351–362, 2010.

Pavel Popela, Jan Novotnỳ, Jan Roupec, Dušan Hrabec, and Asmund Olstad. Two-stage stochastic programming for engineering problems. *Eng. Mech.*, 21(5):335–353, 2014.

Yash Puranik and Nikolaos V Sahinidis. Domain reduction techniques for global NLP and MINLP optimization. *Constraints*, 22(3):338–376, 2017.

Rüdiger Schultz. Continuity and stability in two-stage stochastic integer programming. In *Stochastic Optimization*, pages 81–92. Springer, 1992.

Bernd Stoffel. *Assessing the energy efficiency of pumps and pump units.* Elsevier, 2015.

M. Tawarmalani and N. V. Sahinidis. A polyhedral branch-and-cut approach to global optimization. *Mathematical Programming*, 103:225–249, 2005.

Jess Tindall and Jamie Pendle. Are we significantly oversizing domestic water systems? In *CIBSE Technical Symposium 2015, 16th - 17th April 2015, UCL London.*, 2015.

Jukka Tolvanen. Life cycle energy cost savings through careful system design and pump selection. *World Pumps*, 2007(490):34–37, 2007.

Bogumil Ulanicki, Jens Kahler, and B Coulbeck. Modeling the efficiency and power characteristics of a pump group. *Journal of Water Resources Planning and Management*, 134(1):88–93, 2008.

UN. 2018 revision of world urbanization prospects. Technical report, United Nations, 2018.

Juan Pablo Vielma, Shabbir Ahmed, and George Nemhauser. Mixed-integer models for nonseparable piecewise-linear optimization: Unifying framework and extensions. *Operations Research*, 58(2):303–315, 2010.

Andreas Wächter and Lorenz T Biegler. On the implementation of an interior-point filter line-search algorithm for large-scale nonlinear programming. *Mathematical programming*, 106(1):25–57, 2006.

Jonas B Weber and Ulf Lorenz. Optimizing booster stations. In *Proceedings of the Genetic and Evolutionary Computation Conference Companion*, pages 1303–1310. ACM, 2017.

Jonas B Weber and Ulf Lorenz. Algorithmic system design of thermofluid systems. In *International Conference on Engineering Optimization*, pages 132–143. Springer, 2018.

Roger J-B Wets. Stochastic programs with fixed recourse: The equivalent deterministic program. *SIAM review*, 16(3):309–339, 1974.

Chair of Fluid Systems, Department of Mechanical Engineering, TU Darmstadt, Germany

Email address: {tim.mueller, philipp.leise, imke.lorenz, peter.pelz}@fst.tu-darmstadt.de

Faculty of Energy, Building Services and Environmental Engineering, Münster University of Applied Sciences, Germany

Email address: lena.altherr@fh-muenster.de